NAVAL POSTGRADUATE SCHOOL

MONTEREY, CALIFORNIA

THESIS

FEL MIRROR RESPONSE TO SHIPBOARD VIBRATIONS

by

Joshua A. Beauvais

December 2011

Thesis Advisor:	William Colson
Second Reader:	Keith Cohn

Approved for public release; distribution is unlimited

THIS PAGE INTENTIONALLY LEFT BLANK

REPORT DOCUMENTATION PAGE			Form Approved OMB No. 0704–0188
Public reporting burden for this collection of information is estimated to average 1 hour per response, including the time for reviewing instruction, searching existing data sources, gathering and maintaining the data needed, and completing and reviewing the collection of information. Send comments regarding this burden estimate or any other aspect of this collection of information, including suggestions for reducing this burden, to Washington headquarters Services, Directorate for Information Operations and Reports, 1215 Jefferson Davis Highway, Suite 1204, Arlington, VA 22202–4302, and to the Office of Management and Budget, Paperwork Reduction Project (0704–0188) Washington DC 20503.			
1. AGENCY USE ONLY ***(Leave blank)***	**2. REPORT DATE** December 2011	**3. REPORT TYPE AND DATES COVERED** Master's Thesis	
4. TITLE AND SUBTITLE FEL Mirror Response to Shipboard Vibrations			**5. FUNDING NUMBERS**
6. AUTHOR(S) Joshua A. Beauvais			
7. PERFORMING ORGANIZATION NAME(S) AND ADDRESS(ES) Naval Postgraduate School Monterey, CA 93943–5000			**8. PERFORMING ORGANIZATION REPORT NUMBER**
9. SPONSORING /MONITORING AGENCY NAME(S) AND ADDRESS(ES) N/A			**10. SPONSORING/MONITORING AGENCY REPORT NUMBER**
11. SUPPLEMENTARY NOTES The views expressed in this thesis are those of the author and do not reflect the official policy or position of the Department of Defense or the U.S. Government. IRB Protocol number NA.			
12a. DISTRIBUTION / AVAILABILITY STATEMENT Approved for public release; distribution is unlimited			**12b. DISTRIBUTION CODE** A

13. ABSTRACT

The Optical cavity of a Free Electron Laser (FEL) is composed of components that must be maintained to very tight tolerances. The shipboard environment is one that will preclude a direct coupling of FEL components to the ship. This thesis will explore the basis for these tight tolerances, and how to isolate them from the FEL.

A solid model of a potential FEL system will be developed using SolidWorks. This model will then be converted to a finite element model in ANSYS. The finite element model will be used to calculate the system's eigenvectors. These eigenvectors will be used to develop a state space model in MATLAB. Driving functions simulating sea state 6 and under water explosion will then be applied to the state space model and the motion of various components will be tracked. This simulated motion will be used to develop and test a passive control system to damp out the vibrational input to the FEL.

It is not possible for a passive system to totally isolate the FEL from excitation by the ship environment. A passive system that minimizes the inputs to an active control system will be developed. An active system that will handle the final mirror stabilization for a FEL optical cavity will be left for further research.

14. SUBJECT TERMS Free Electron Laser, FEL, Vibration, Finite Element, Shipboard Vibration, Passive Control, Oscillator, Mirror Alignment, Resonator Alignment			**15. NUMBER OF PAGES** 77
			16. PRICE CODE
17. SECURITY CLASSIFICATION OF REPORT Unclassified	**18. SECURITY CLASSIFICATION OF THIS PAGE** Unclassified	**19. SECURITY CLASSIFICATION OF ABSTRACT** Unclassified	**20. LIMITATION OF ABSTRACT** UU

NSN 7540–01–280–5500 Standard Form 298 (Rev. 2–89)
Prescribed by ANSI Std. 239–18

THIS PAGE INTENTIONALLY LEFT BLANK

Approved for public release; distribution is unlimited

FEL MIRROR RESPONSE TO SHIPBOARD VIBRATIONS

Joshua A. Beauvais
Lieutenant, United States Navy
B.S., Worcester Polytechnic Institute, 2003

Submitted in partial fulfillment of the
requirements for the degree of

MASTER OF SCIENCE IN APPLIED PHYSICS

from the

NAVAL POSTGRADUATE SCHOOL
December 2011

Author: Joshua A. Beauvais

Approved by: William Colson
Thesis Advisor

Keith Cohn
Second Reader

Andres Larraza
Chair, Department of Physics

THIS PAGE INTENTIONALLY LEFT BLANK

ABSTRACT

The Optical cavity of a Free Electron Laser (FEL) is composed of components that must be maintained to very tight tolerances. The shipboard environment is one that will preclude a direct coupling of FEL components to the ship. This thesis will explore the basis for these tight tolerances, and how to isolate them from the FEL.

A solid model of a potential FEL system will be developed using SolidWorks. This model will then be converted to a finite element model in ANSYS. The finite element model will be used to calculate the system's eigenvectors. These eigenvectors will be used to develop a state space model in MATLAB. Driving functions simulating sea state 6 and under water explosion will then be applied to the state space model and the motion of various components will be tracked. This simulated motion will be used to develop and test a passive control system to damp out the vibrational input to the FEL.

It is not possible for a passive system to totally isolate the FEL from excitation by the ship environment. A passive system that minimizes the inputs to an active control system will be developed. An active system that will handle the final mirror stabilization for a FEL optical cavity will be left for further research.

THIS PAGE INTENTIONALLY LEFT BLANK

TABLE OF CONTENTS

LIST OF FIGURES

LIST OF TABLES

THIS PAGE INTENTIONALLY LEFT BLANK

LIST OF ACRONYMS AND ABBREVIATIONS

cryo	Cryogenic
FEL	Free Electron Laser
JLab	Thomas Jefferson National Accelerator Facility
RF	Radio Frequency
Hz	Hertz
SS-6	Sea State 6
UW	Underwater
SCA	Superconducting Accelerator
AES	Advanced Energy Systems

THIS PAGE INTENTIONALLY LEFT BLANK

ACKNOWLEDGMENTS

I want to extend my thanks to all who helped me in this process: Professors Bill Colson and Keith Cohn, at the Naval Postgraduate School, and Professional Engineer Mike Hatch of M.R. Hatch Consulting.

THIS PAGE INTENTIONALLY LEFT BLANK

I. INTRODUCTION

A. BACKGROUND

There are several distinct combat scenarios where the free electron laser (FEL) will be of great benefit to the Navy. For example, the FEL can become a ship's primary self-defense weapon against inbound airborne threats, but can also provide a less-than-lethal means of deterring small craft, and can be used for a precision strike against shore targets near the coastline.

1. Free Electron Laser for Self Defense

a. Aircraft

The FEL has the capability to project energy long distances at the speed of light. A megawatt class FEL will also be capable of destroying enough material in about one second to render a target missile incapable of flight. Other types of aircraft will require more or less time on target depending on their construction. The laser is also capable of retargeting nearly instantly since the beam director need only be aligned to the new target. Unlike some other high power lasers, the FEL does not have a required cooling time between or after a certain number of shots.

b. Waterborne Threats

The optical targeting of the FEL is expected to be accurate enough to enable it to be used against small craft in a number of ways. It can be used at lower power settings to cause small amounts of damage to the craft as a sort of a warning shot. It also can be used to make holes in the hull near the waterline or to disable the engines.

2. Shore Engagements

Some targets on shore can be disabled or destroyed by the loss of a small amount of material. Since the operation of the FEL only requires electricity, the only cost in its use is ship's fuel. The "pinpoint" accuracy of the system allows for engagements that would have been unfeasible with any other system based on a cost benefit analysis.

B. SENSITIVE COMPONENTS

The many benefits of the FEL system come at a non-trivial cost. The system is costly but it is not likely to be any more so than other weapon systems of equal power. Any system that works with megawatts of power is composed of many sensitive components with tight tolerances; the FEL is no exception. The laser is quite large and has components that must be aligned within microradians and must also have their separation maintained within micrometers. The operating environment may be one which vibrates with significant amplitude over a broad spectrum of frequencies. Achieving either of these conditions would be no small feat in a shipboard environment; the FEL requires both.

C. SCOPE OF RESEARCH

The system to maintain tolerances on the FEL will necessarily be one that is quite sophisticated. The scope of this thesis will be limited to the alignment of three important components: the two optical resonator mirrors, and the electron beam. This project will model the whole FEL system, simulate that model in a shipboard vibrational environment, develop a passive isolation system to minimize vibrational input, and establish the boundary conditions for an active control system to stabilize these three components.

II. FREE ELECTRON LASER SYSTEM

A. COMPONENTS

The Free Electron Laser (FEL) is comprised of several main types of components. These components range from bending magnets to superconducting linear accelerators. A complete assembly of these components is in Figure 1. The figures in this section are for illustrative purposes only; this model is a notional design that captures the mechanical properties of various FEL components for the purpose of studying the effects of a vibrating environment on the system.

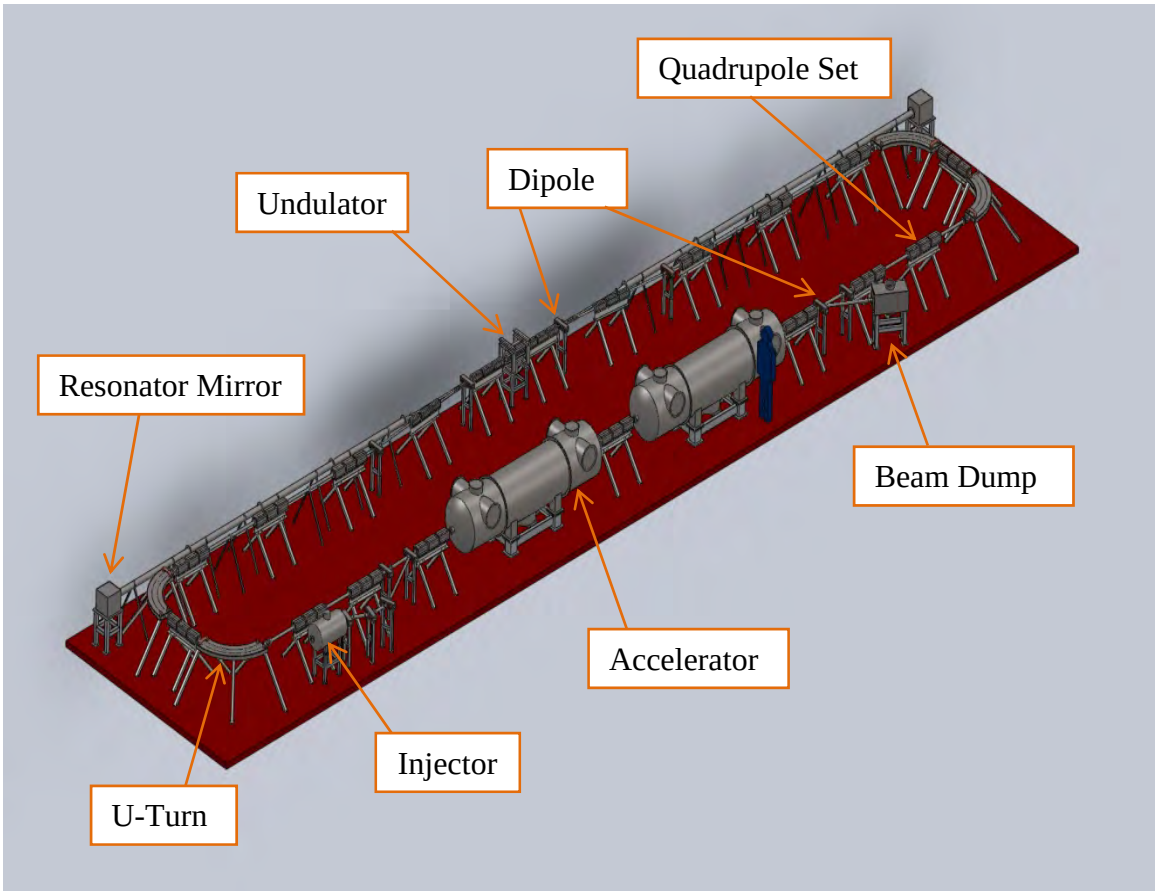

Figure 1: FEL Solid Model

1. Injector

The injector, an example of which is in Figure 2, is a source of electrons. In this case they are generated by a short pulse length laser that is impinging on a photo cathode. The laser pulses used to generate the photoelectrons in the photocathode are synchronized with the radio frequency (RF) field in the injector cavity to produce positive acceleration to the electrons. These electron bunches are also produced in phase with the RF Field in the main accelerator so that their energy can be further increased. The injector requires vacuum, RF power, and cooling systems in addition to the seed laser to support its operation. The injector, as well as the entire beam line, requires extremely high vacuum; approximately 10^{-10} Torr is necessary to prevent unwanted electron scattering, and cathode degradation.

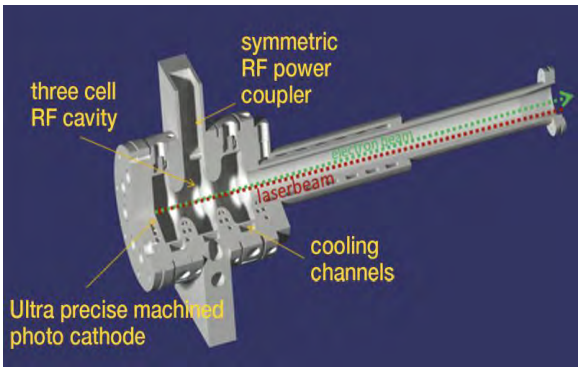

Figure 2: Injector Cutaway. From [1]

2. Accelerator

The accelerator uses an RF power source to establish an oscillating electromagnetic field inside a series of cavities such as those pictured in Figure 3. This field will incrementally, depending on phase relation, accelerate or decelerate a bunch of electrons as they pass through each cavity. The phase relationship between acceleration and deceleration allows for energy recovery with a recirculating beam line. In this model, the accelerator cavities are superconducting devices operating at 2K. Working at this temperature requires additional support systems using liquid helium. The thermal insulation for this device will be accomplished in steps. The 2K volume will be surrounded by an insulating vacuum, outside this vacuum layer is a 77K liquid nitrogen

layer, next is another insulating vacuum, finally a typical thermal insulation is used. The insulating vacuum is not required to be of the same quality as the beam line and is only held at approximately 10^{-4} Torr. The accelerator cavities however, being part of the beam, contain the same 10^{-10} Torr vacuum as the injector.

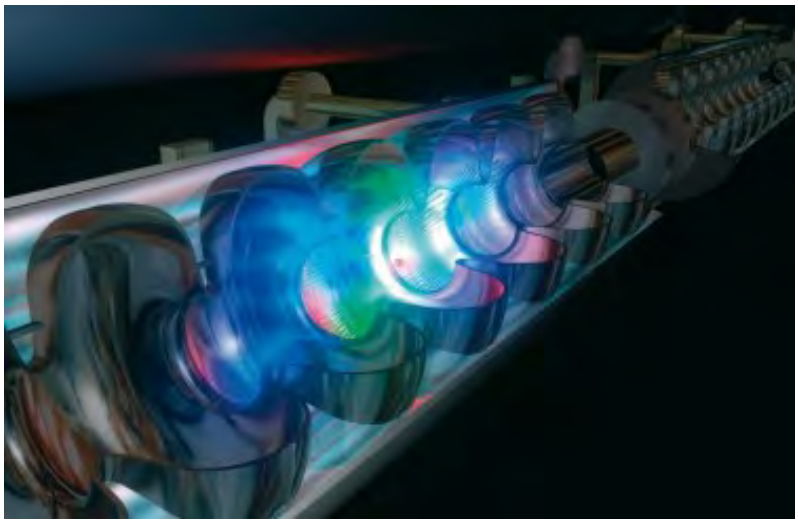

Figure 3: Accelerator Cutaway. From [2]

3. Bending Magnets

There are several types of bending magnets that may be used in the FEL. In this design, there is a smaller dipole merge magnet, and a much larger magnet for turning the beam around creating the recirculating loop.

a. Dipole

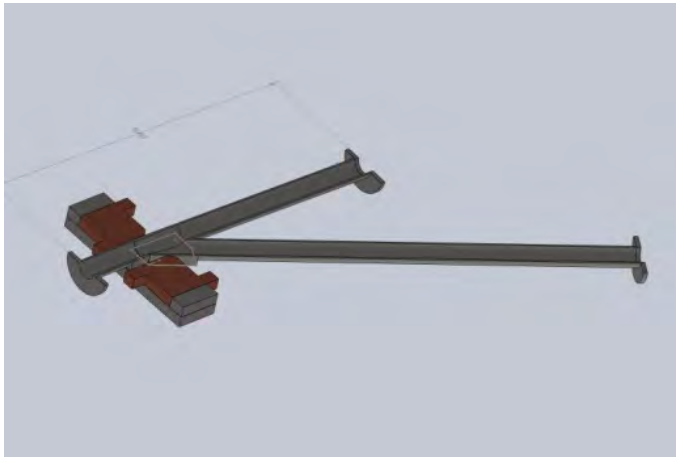

Figure 4: Cross Section View of a Dipole Magnet with Attached Piping and Windings Shown in Brown

The smaller dipole magnets cause a bend radius that is proportional to charge, energy, and magnetic field. A cross section view of this type of magnet can be seen in Figure 4. In the figure, the grey material is steel and the brown is copper simulating the windings for this electro-magnet. These colors are constant throughout the SolidWorks [3] model and will not be described again. These magnets are used in 4 places in this FEL design: (1) They interlay low and high energy electron bunches at the outlet of the injector so that they enter the accelerator along a common beam line axis but at different RF phases, (2) they separate low and high energy electron bunches at the outlet of the accelerator so that the high energy electrons travel down the main beam line and the low energy ones enter the beam dump, they also allow the optical beam and electron beam to (3) enter and (4) exit the optical cavity. For this model, the same magnets are used with a slightly different piping arrangement to deflect the electron beam and, where necessary, to align it for travel through downstream components.

b. U-Turn

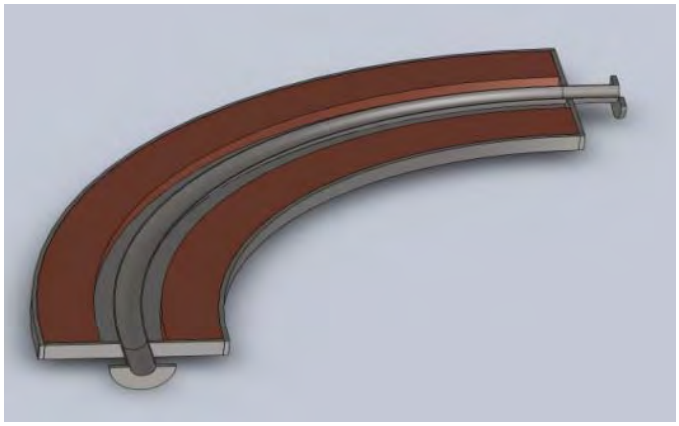

Figure 5: Cross Section View of a U-Turn Magnet with Attached Piping and Windings Shown in Brown

Large 90˚ dipole bending magnets are used at opposite ends of the electron beam line to create the loop that allows for energy recovery in a recirculating FEL. A cross section view of one of these magnets can be seen in Figure 5. Two of the 90˚ magnets are used in conjunction with a focusing magnet to turn the beam a full 180˚.

4. Focusing Magnets

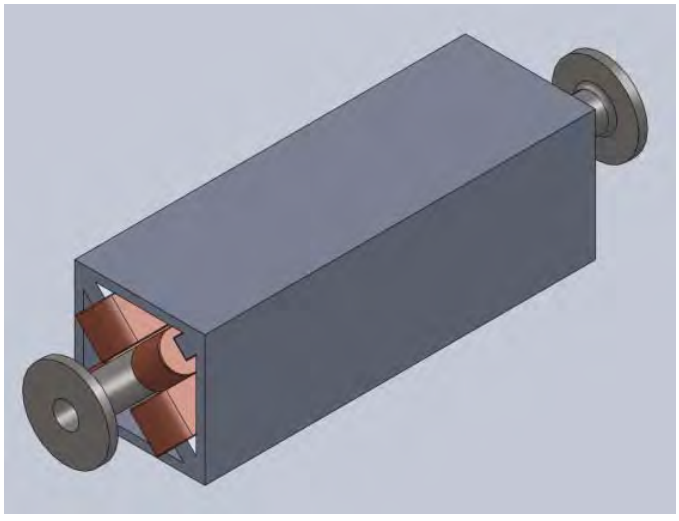

Figure 6: Quadrupole Focusing Magnet with Attached Piping and Windings Shown in Brown

Quadrupole focusing magnets are used to focus the electron beam radially at various locations around the beam line. These magnets are used in 19 locations along the beam line to maintain the approximately 1 millimeter beam envelope radius. This model uses these magnets in sets of three to balance the induced angular spreads in both of the transverse directions being controlled. An example of one quadrupole magnet can be seen in Figure 6.

5. Undulator

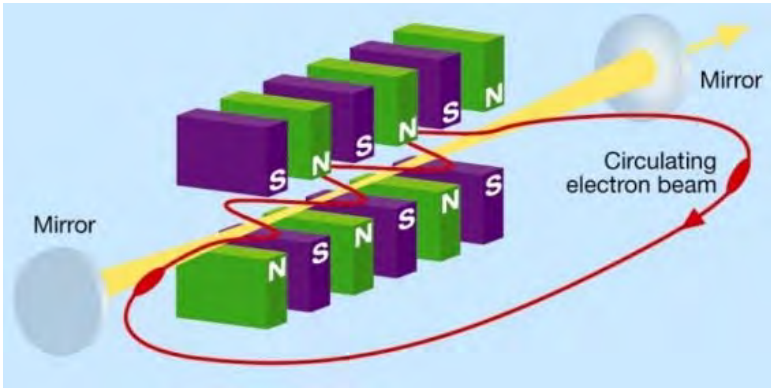

Figure 7: Undulator Principle. From [4]

The linear undulator is a device that contains a set of magnets whose poles alternate between north and south along the long axis of the undulator. An example is sketched in Figure 7. The alternating of poles sets up a sinusoidally varying magnetic field that will, via the Lorentz Force, cause the electron beam to travel in a sinusoidal path. The acceleration associated with a sinusoidal trajectory will cause the electron beam to emit synchrotron radiation.

6. Beam Dump

The beam dump is a large block of copper surrounded by shielding. Its purpose is to capture the electrons that come out of the accelerator at about 5 MeV and then to shield the radiation produced by the copper-electron interaction. The beam dump must also be cooled as it will need to dissipate about five megawatts of heat generated by stopping the electrons.

7. Resonator Mirrors

The navy FEL may be an oscillator design, as is considered here. This design will use a pair of resonator mirrors set up to reflect light pulses through the undulator in synchronism with the electron pulses. Furthermore, one of the mirrors will be partially transparent to allow for usable light to "leak" out of one end. These mirrors will need to be a significant distance apart to allow for sufficient spreading of the optical beam to prevent distorting or damaging the mirrors. It is this distance and the sensitivity of the alignment with the electron beam in the undulator that this project will be exploring.

B. OPERATION

Electrons are liberated from the cathode in the injector in bunches with charge of about one nanocoulomb at a rate of 750 MHz, resulting in approximately one ampere of current. These bunches are then accelerated to about five MeV in the injector, and sent to the accelerator. In the accelerator, the electrons enter in phase with the oscillating RF field, where their energy is increased to about 100 MeV. The electrons then travel through a series of focusing and bending magnets along their path to the undulator. The sinusoidally varying magnetic field in the undulator will cause a periodic acceleration due to the Lorentz force. The electrons will be directed off on their trajectory in the plane normal to the magnetic field in a sinusoidal path; this transverse acceleration causes the electrons to interact with the laser field in the resonator and transfer a few percent of their energy to the light. The electrons then travel through another series of bending and focusing magnets on their trip back to the accelerator. This time, the bunches of electrons enter the accelerator 180˚ out of phase and are decelerated so that the high energy electrons give up most of their energy to the RF Field. This both reduces the required RF energy input to the accelerator, and drastically lowers the radiation and heat produced in the beam dump.

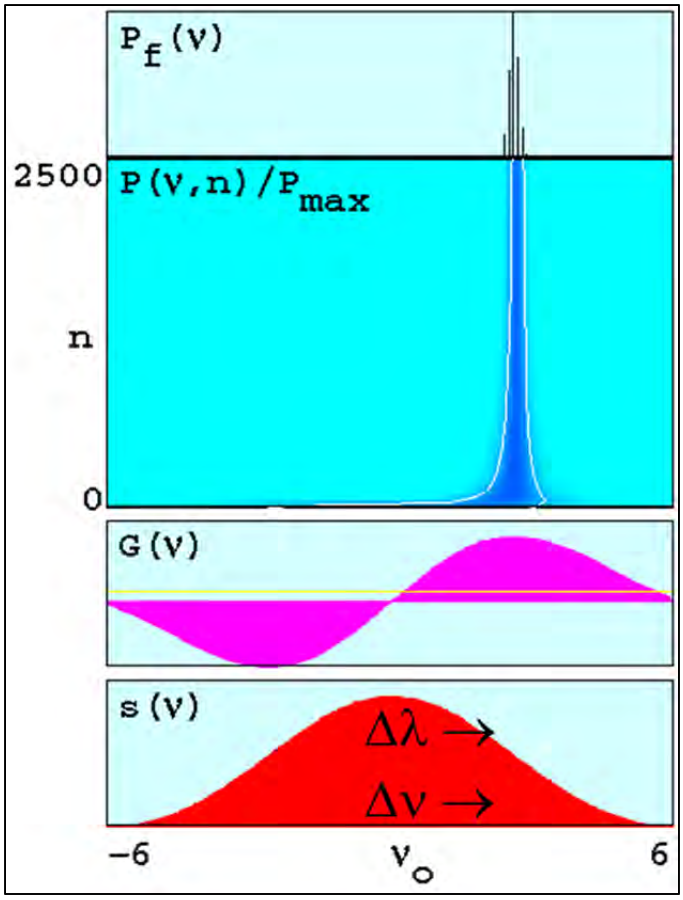

Figure 8: **FEL Power, Gain, and Optical Spectrum vs. Frequency for 2500 Passes through the Undulator. From [5]**

This interaction allows the light to become coherent at a specific frequency over a large number of passes through the undulator. The interaction occurring many times also allows for high power to be developed in the optical beam. Figure 8 demonstrates the development of the optical mode in this type of FEL. The typical gain spectrum is shown in purple, as a function of wavelength, with higher gain above the zero line. The gain spectrum plot also shows the threshold for continuous operation in yellow, gain above this line is necessary to make up for the energy extracted. The blue plot shows the evolution of the power spectrum of the optical mode for each pass over 2500 passes with darker blue indicating more optical power. Finally, the power spectrum at the end of the

2500 passes is shown in black. The simulation is started with the spontaneous optical spectrum (red) and the spectrum rapidly narrows to a very small bandwidth. This process happens quickly in the time domain:

However, the electrons must be able to repeat the process with high accuracy and repeatability several thousand times.

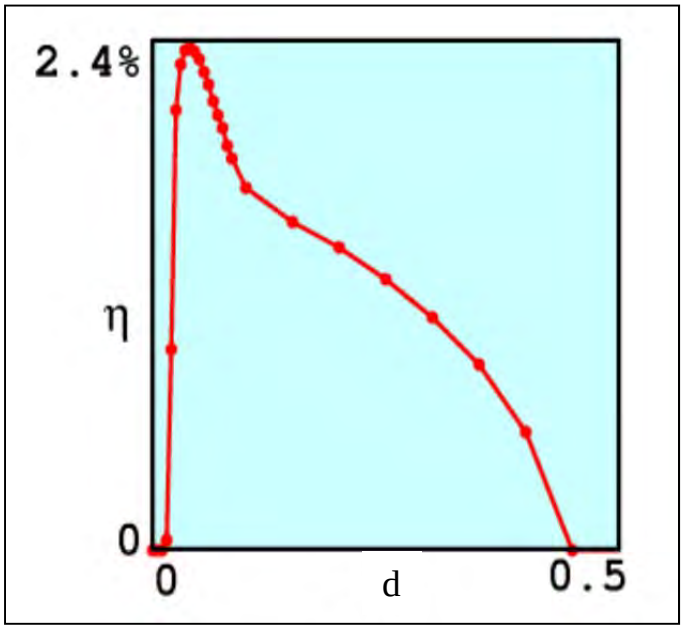

Figure 9: FEL Extraction (η) vs. Desynchronism (d). From [5]

The light produced in the undulator is stored between the two resonator mirrors, and is amplified each pass through the undulator. In order for this amplification to occur, the distance between the mirrors must be set so that the arrival of the optical pulse is synchronized with the arrival of an electron pulse so that they enter the undulator together. Figure 9 shows a plot of FEL extraction percentage (η) vs. the range of mirror positions ΔS quantified by the dimensionless desynchronism parameter .
One of the mirrors is moved closer to the undulator by the distance ΔS in order to account for optical lethargy [5]. This ensures that the two pulses arrive in synchronism many times and allows for coherence and high power to be developed in the optical beam.

From Figure 9, the range of possible values for d is about 0.45 in this example. Assuming an optical wavelength of $\lambda = 1\,\mu m$, and the number of periods in the undulator is N = 20, the mirror can change by about $\Delta S = d * N\lambda/2 = 0.45 * 20\mu m/2 = 4.5\mu m$ before this representative system stops working.

C. SYSTEM TOLERANCES

In the shipboard environment, vibrations from various sources can cause fluctuations in the separation and alignment of the resonator mirrors. From the calculation of ΔS above, one of the tolerances on the position keeping of the resonator mirrors can be determined. Moving one mirror through a range of $5\mu m$ takes the laser from not working, to producing max power, to not working again. This large a swing in output power is not acceptable for FEL operation; the extraction needs to be better controlled. Because both mirrors move, each must be maintained within about $1\mu m$ to maintain approximately constant extraction. Setting the starting position of each mirror at the center of its band, the tolerance on position in this direction is $\pm 0.5\mu m$.

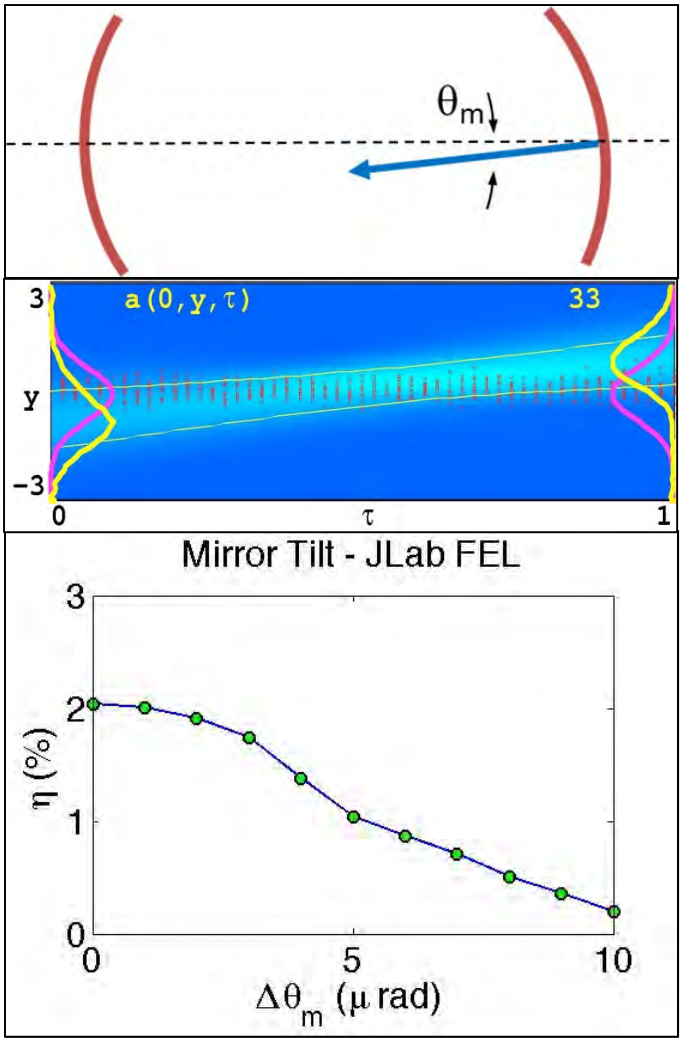

Figure 10: FEL Extraction vs. Mirror Tilt Study Performed on a Power Upgrade to the JLab FEL. From [6]

A study of mirror tilt was also performed at NPS on a Thomas Jefferson National Accelerator Facility's (JLab) FEL [6] and the results are shown in Figure 10. The top sketch shows θ_m as the angle between the long axis of the undulator and the mirror being rotated. The middle plot shows the electron beam (red), the electron pulse shape (purple), the optical mode at the beginning and end of the undulator (yellow), and the size and shape of the resulting optical beam (light blue) for a deflection of 5 microradians. The resulting FEL extraction is shown in the bottom of Figure 10 as a function of θ_m. Of note, this study showed that a mirror tilt of only 5 microradians produced a tilt in the optical mode of 1 milliradian and a reduction of laser power by a factor of two. This

serves to emphasize why controlling the mirror angle so tightly is both important and necessary for FEL operation. These results establish two new tolerances on the resonator mirrors that will be explored in this project, the angle of the two resonator mirrors must be maintained within about ±5 microradians, and the optical mode rotation must be maintained within about ±1 milliradian.

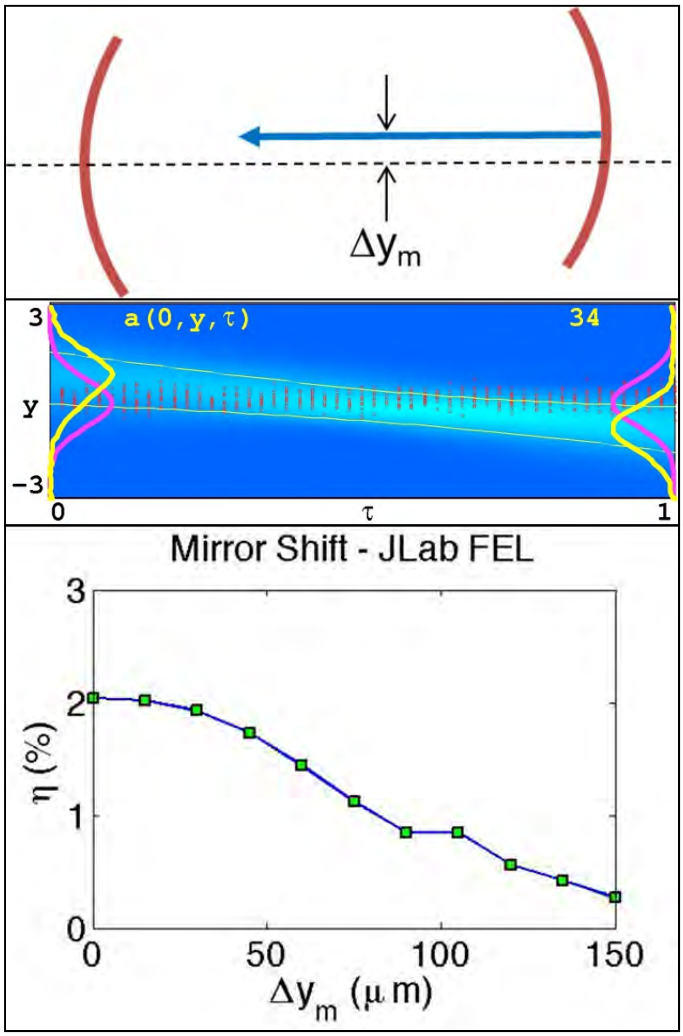

Figure 11: FEL Extraction vs. Mirror Shift Study Performed on a Power Upgrade to the JLab FEL. From [6]

To predict the effects of mirror shift, another study was performed on JLab's FEL in [6], as shown in Figure 11. The top sketch shows ΔY_m as the distance between the long axis of the undulator and the center of the mirror being displaced. The middle plot shows the electron beam (red), the electron pulse shape (purple), the optical mode

(yellow), and the size and shape of the resulting optical beam (light blue) for a deflection of 75 micrometers. The resulting FEL extraction is shown in the bottom of Figure 10 as a function of ΔY_m. This 75 micrometer shift also produces an optical mode rotation of 1 milliradian and lowers extraction by a factor of two. From these results, a tolerance of $\pm$50 micrometers is established on resonator mirror shift and the ±1 milliradian tolerance on optical mode rotation is reinforced.

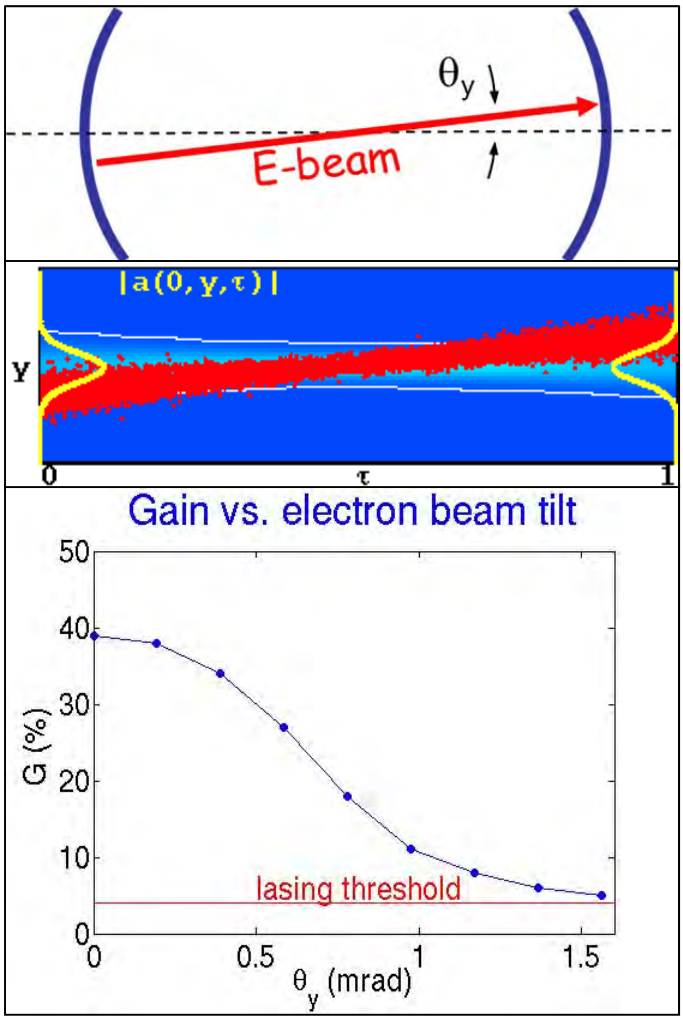

Figure 12: Gain vs. Electron Beam Tilt Setup. From [5]

Another similar study of was performed [5] focusing on electron beam tilt in a typical FEL as shown in Figure 12. The top sketch shows θ_y as the angle between the optical mode and the electron beam. The middle plot shows the electron beam (red), the

ideal Gaussian shaped optical mode (yellow), the size and shape of the optical beam (light blue), for an angle θ_y between the optical mode and electron beam. This study worked on the premise that prior to entering the undulator, the electron beam was deflected out of alignment with the optical resonator. The result was a loss of optical weak field gain, shown in the bottom figure, since the two beams were not always collocated. If there is no light present near the electron beam, stimulated emission cannot occur and there will be reduced gain in that region. Without adequate gain, the FEL will be unable to start up. If it is assumed that the electron beam travels through the center of the undulator, as designed, then a logical extension of this study is that if the optical beam is out of alignment by the same angle as the electron beam in this study, the same results will occur. At about one milliradian of optical beam misalignment the laser loses 75 percent of its weak field gain and becomes unlikely to start up. The mirror alignment required for FEL startup is ±0.5 milliradians.

In [7], a simulation of JLab's FEL oscillator was performed to determine constraints on energy extraction (η) from the electron beam due to its shift (Δy) and tilt ($\Delta\theta_y$) together relative to the undulator axis as shown in Figure 13. Maintaining extraction at approximately two percent is estimated as necessary to generate the useful optical power that the FEL is intended to produce. For the same reasons as before, both the angular and shift results for the electron beam can be applied to the optical beam. The optical beam angle must be controlled to within 1 milliradian. Another new tolerance on mirror motion emerges from this data, the optical beam and thus the optical mode shift must be controlled to ±0.6 millimeters.

The tolerances developed in this chapter are summarized in Table 1.

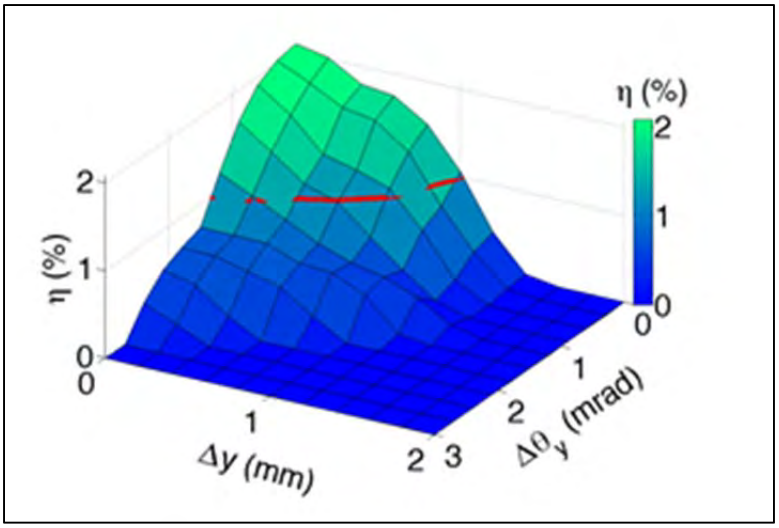

Figure 13: Extraction vs. Electron Beam Shift and Tilt. From [7]

Table 1: FEL System Tolerances

Dimension to be Controlled	Tolerance
Mirror Angle	±0.5 microradians
Mirror Shift	±50 micrometers
Optical Path Angle	±1 milliradian
Optical Path Shift	±0.6 millimeters
Mirror Separation	±0.5 micrometers

THIS PAGE INTENTIONALLY LEFT BLANK

III. MODELING

A. SOLID MODEL

The modeling began with the development of a solid model of a notional FEL oscillator system using SolidWorks. A tour of the now disassembled Superconducting Accelerator (SCA) FEL at Stanford University was taken to familiarize the designers with the components of the system, and their construction.

The first step in the design process was to develop a table of masses of components from several existing models; see Table 2. The three columns from Advanced Energy Systems (AES) are different power levels that were presented in [5]. The FELSIM [8] column is based on a megawatt class laser simulation. Where information was not available, masses were developed using common engineering materials and approximate dimensions of components. Using the data compiled, and standard engineering materials, a solid model of a notional FEL system was developed. There are two places where the constructed model for this project differs greatly from the data collected. The injector modeled is a superconducting quarter wave gun being developed by Niowave, Inc. in Lansing, MI. The second deviation is that this model is using a half meter permanent magnet undulator. Both of these designs are much less massive than their traditional counterparts. The exact properties of the system with regards to the functionality of the laser itself are not critical to this project. What is important, and what is being emphasized in this model, is that individual mass, moment of inertia, and stiffness for various components be consistent with a possible configuration for a FEL system. A three dimensional rendering of the solid model can be seen in Figure 1 above.

Table 2: Component Mass Comparison from Other Models

Component	AES Model #1 mass (kg total)	AES Model #2 mass (kg total)	AES Model #3 mass (kg total)	FELSIM 90kW (kg each)	Model Average	Selected Project Model mass (kg each)
Photocathode Laser	250	450	704	*	468	⋆
Injector	2700	2900	4000	1171	2693	173
Dipole	*	*	*	37	37	50
Quadrupole magnet	*	*	*	262	262	269
LINAC	2350	1900	1900	2121	2068	1717
Beam dump	400	1300	2300	*	1333	787
90° Dipoles	*	*	*	*	*	360
Undulator	1000	800	800	317	729	100
Mirror Assembly	*	*	*	*	*	118
optical path	*	*	*	500	500	843
Cryo system	14000	13000	10000	*	12333	⋆
RF Sources	1100	8100	20000	*	9733	⋆
RF distribution	2400	5400	13000	*	6933	⋆
HVDC power supply	2000	4000	12000	*	6000	⋆
Total System Mass (Tons)	55	67	85	36.2	61	40.5

* Data Not Available ⋆ Component not Included in Model

B. ANSYS MODEL

In order to facilitate simulations, a finite element model based on the solid model needs to be created. A solid model of a system such as this contains a huge amount of data. There are techniques to generate a finite element mesh directly from the solid model; however, the matrices associated with them become quite large and are prone to errors and long processing times. To avoid the long simulation times and possibly inaccurate results, a beam element based finite element model was developed using ANSYS [9]. The finite element model is one that is effectively composed of sticks and masses. This model uses the spatial properties of the solid model and joins them with linear elements that have the same mass and inertial properties as the bodies developed in the solid model. Top views of both models can be seen below in Figure 14 to illustrate both the geometric similarity between the two models and how drastically simplified the finite element model (top) is as compared to the solid model (bottom). As drastic as this simplification is, there is no loss in the how the model behaves globally, only in how it is processed in the simulation.

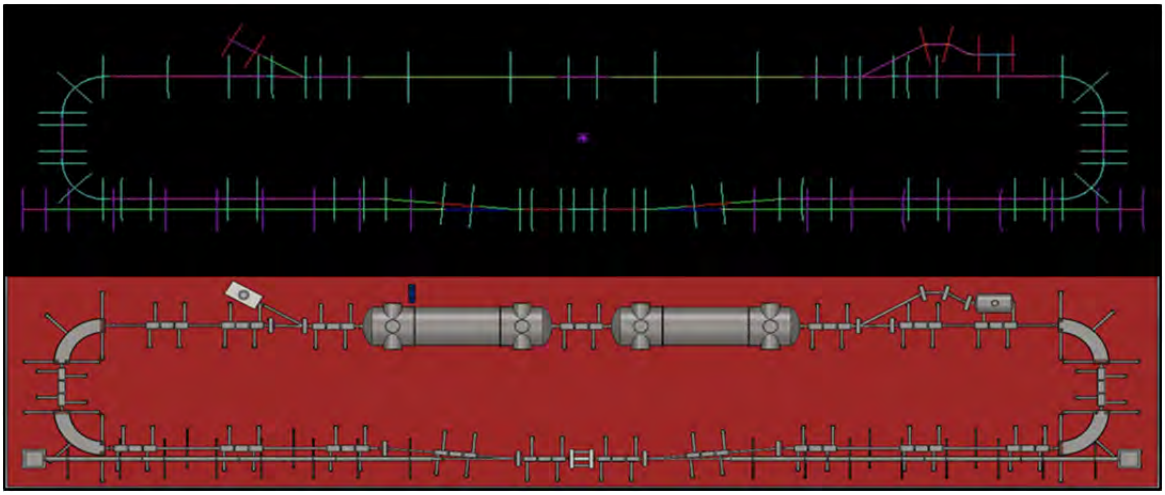

Figure 14: Finite Element model (top), Solid Model (bottom), The Details of the Solid Model are Shown in Figure 1

1. Element Development

The reason that there is no loss in fidelity with the finite element model is because of the way the elements are programmed, and the questions asked of the simulation. Each element has two sets of properties associated with it, one for material properties, and one for inertial properties. The set of material properties contains three values: Young's modulus, Poisson's ratio, and the density. The set of inertial properties for the structural beam element used in this model contains 12 values: cross-sectional area, area moment of inertia in all three directions, thickness in both cross-sectional directions, orientation angle of the element, shear modulus, and others that are not used in this model.

These values are obtained in one of two ways. If the component being modeled is made of a single uniform material then the general material property values can be looked up in a handbook and the other properties can be measured off of the solid model. If the component is a composite or has a non-uniform cross section, then an average value must be determined for that component. A dimensioned cross section of a quadrupole magnet is shown in Figure 15; example composite body calculations of area moments of inertia and density follow, using standard formulas and the parallel axis theorem. All dimensions in Figure 15 are in meters and directly translate into the formulas following the figure.

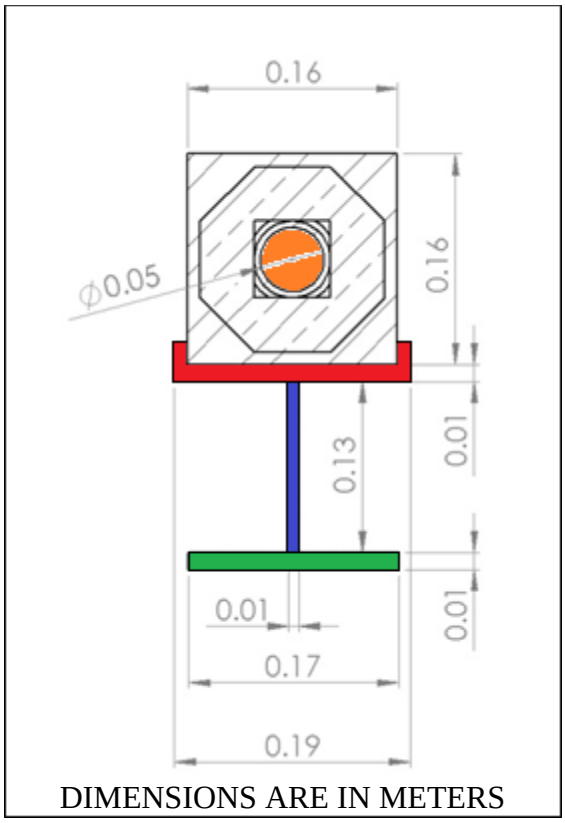

Figure 15: Quadrupole Magnet Dimensioned Cross Section

$$I_{yy} = \underbrace{\frac{0.16^3 * 0.16}{12}}_{\text{White}} - \underbrace{\frac{\pi * (0.05/2)^4}{4}}_{\text{Orange}} + \underbrace{\frac{0.01^3 * 0.19}{12} + 0.01 * 0.19 * 0.085^2}_{\text{Red}}$$
$$+ \underbrace{\frac{0.13^3 * 0.01}{12} + 0.01 * 0.13 * 0.155^2}_{\text{Blue}} + \underbrace{\frac{0.01^3 * 0.17}{12} + 0.0017 * 0.225^2}_{\text{Green}}$$
$$= 1.87\text{x}10^{-4}\text{m}^4$$

$$I_{zz} = \underbrace{\frac{0.16^3 * 0.16}{12}}_{\text{White}} - \underbrace{\frac{\pi * (0.05/2)^4}{4}}_{\text{Orange}} + \underbrace{\frac{0.19^3 * 0.01}{12}}_{\text{Red}} + \underbrace{\frac{0.01^3 * 0.13}{12}}_{\text{Blue}} + \underbrace{\frac{0.17^3 * 0.01}{12}}_{\text{Green}}$$
$$= 6.41\text{x}10^{-5}\text{m}^4$$

Mass = 237.33 kg
Volume = .0287 m^3
Length = 0.98 m

$$\text{Linear Density} = \frac{237.33\ \text{kg}}{.0287\ \text{m3} * 0.98\ \text{m}} = 8.438$$

All of the other properties for these elements are similarly calculated.

2. Eigenvectors and Eigenvalues

Based on the elements data, and geometry entered, ANSYS produces an output file that contains the eigenvalues, and eigenvectors of oscillation for the first 50 vibrational modes of the system. These eigenvalues are the natural frequencies for each of the modes and the eigenvectors are the shapes of each of the modes. This file will then be imported into MATLAB for further processing and application of a driving function.

C. SEA SIMULATION

The sea input to the model was approached in two ways; a steady state input representing a series of waves and a shock input. For the purposes of this project, a DDG-51 class ship will be used as the vessel to carry the FEL. It is likely that this is the smallest ship that would carry an FEL. Furthermore, and any effect calculated for this hull form would be reduced on any larger vessel. As such, if the system can be maintained in alignment on the DDG, it should be similarly possible on any larger ship. The worst-case sea state in which an engagement is likely to occur is sea state 6 (SS-6), from Table 3. Seas of 4 to 6m will be used in determining the steady state driving function for the model.

Table 3: Table of Sea States. From [10]

Sea State	Description	Wave Height (m)
0	Calm (glassy)	0
1	Calm (rippled)	0–0.1
2	Smooth (wavelets)	0.1–0.5
3	Slight	0.5–1.25
4	Moderate	1.25–2.5
5	Rough	2.5–4
6	Very rough	4–6
7	High	6–9
8	Very high	9–14
9	Phenomenal	over 14

Data from an underwater (UW) explosion was recorded during the shock trials of USS Winston S. Churchill and can be seen below in Figure 16. This will be approximated as a 45g, 4ms half sine pulse and applied to the model to explore how the system responds to shock loading from an underwater explosion.

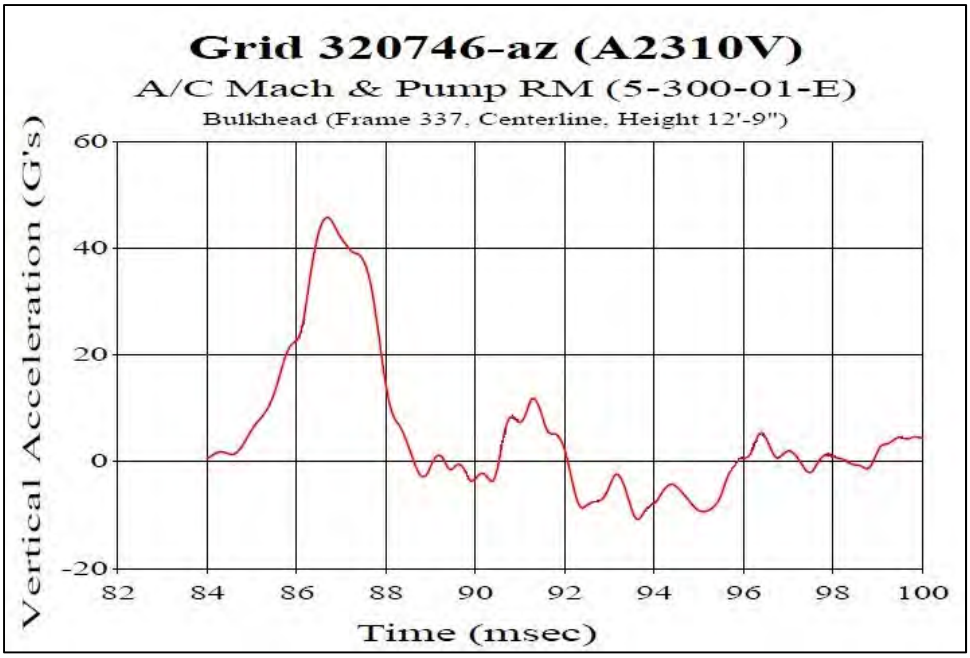

Figure 16: Shock Trials Data for USS Winston S. Churchill. After [11]

The DDG-51 hull form was entered into SHIPMO [12], a program that tracks a ship's 6 degrees-of-freedom at various speeds and relative courses. MATLAB [13] was used for post processing of this data and polar plots of the resulting peak vertical acceleration and period for sea state 6 are below in

Figure 17. In the figure, relative bearing to the seas is shown azimuthally, with 180° indicating that the ship's heading is directly into the seas, and the ship's speed increasing radially from zero at the center to 30 knots moving outward. Considering the vibration isolation strategy that will be used, the worst inputs would be the highest amplitude for acceleration and the lowest period for that acceleration. As it turns out, these two conditions coincide at a single point, 30 knots with the ship's heading directly into the seas. A worst-case steady state sinusoidal driving function of 0.12g in amplitude and a period of 5 seconds were determined.

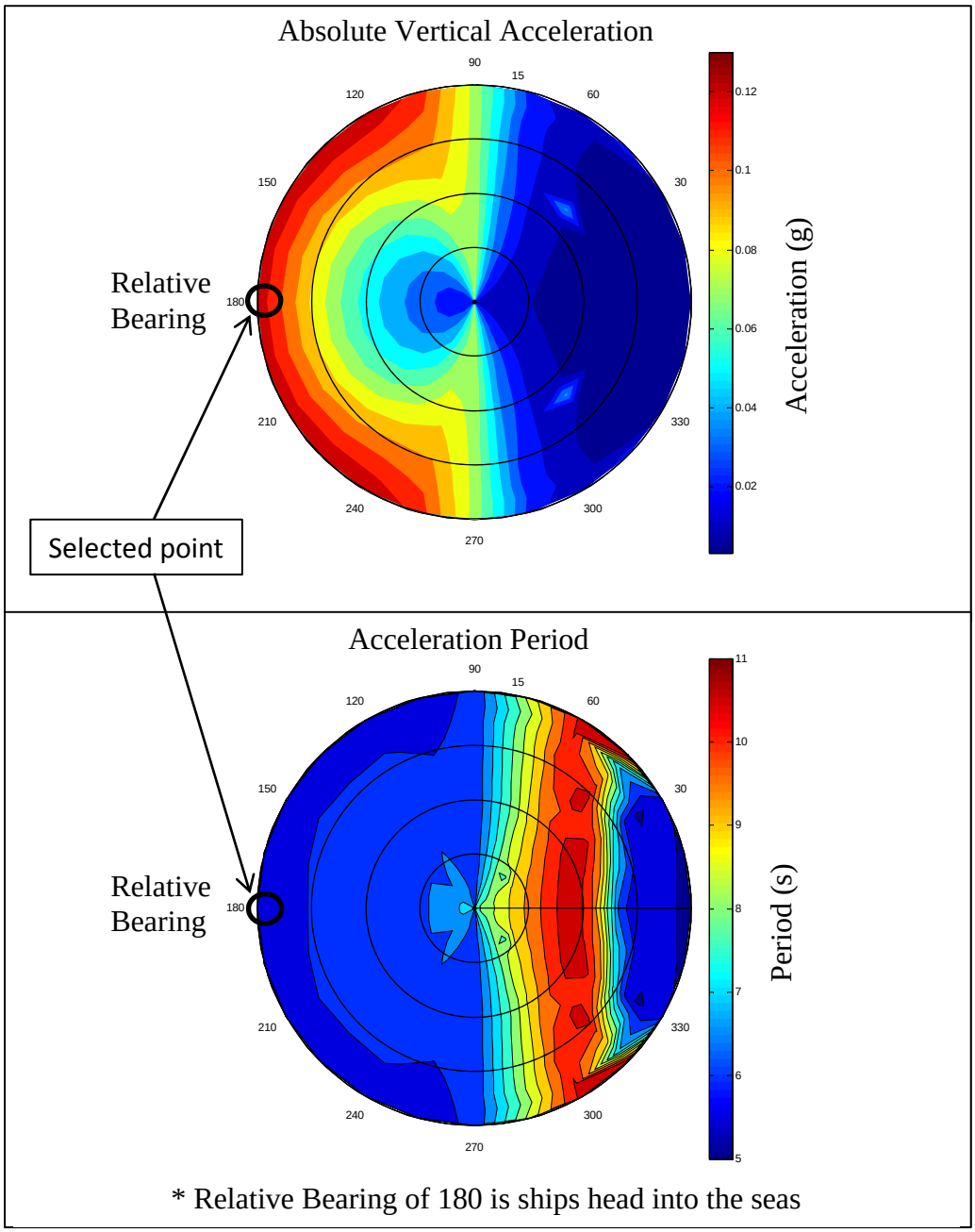

Figure 17: **Vertical Acceleration and Period for SS-6 Plotted Azimuthally vs. Ship's Heading and Radially vs. Ship's Speed**

D. STATE-SPACE MODEL AND ANALYSIS

MATLAB is used to perform a series of calculations. First, it is used to convert the eigenvectors and values into a state-space model. The state-space model is a frequency domain model that is used to calculate transfer functions for the various components being tracked. An example transfer function is below in Figure 18, showing how the undulator and mirrors respond to input frequencies between 0.1 and 100 Hz. For illustrative purposes some of the various vibrational inputs to the system have been indicated in their relative frequency range.

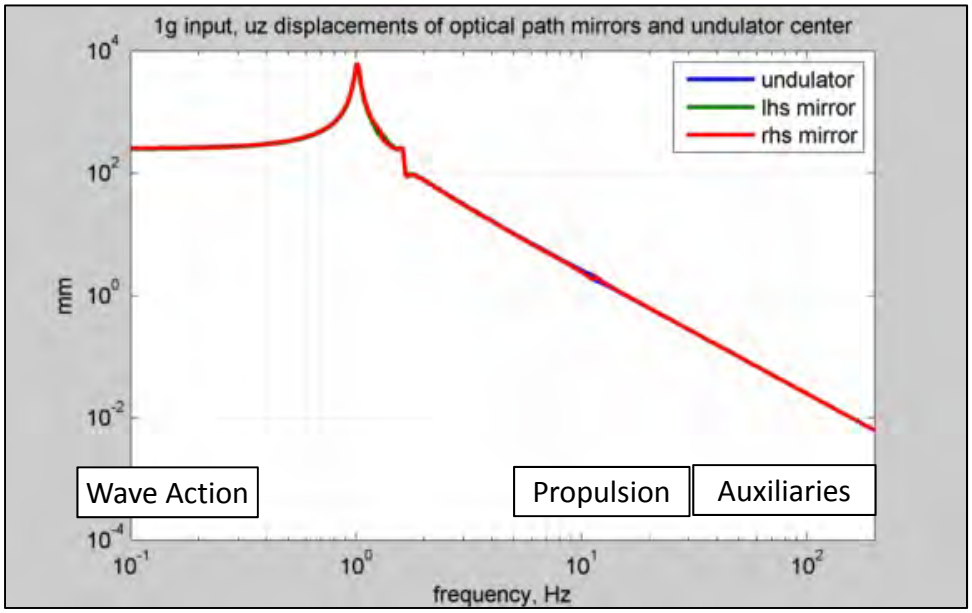

Figure 18: Example Transfer Function for Resonator Components

The state space model is then converted into a time domain system model to allow for the computation of actual displacements and time histories in response to a driving function. An example motion plot is below in Figure 19; the figure shows the response in the vertical, (Z) direction, of a preliminary model that has four springs at the outer corners, from a continuous sine wave input. This time domain model also allows for the

comparison of motion between any of the components in the FEL system in any direction and will be the primary design tool for optimizing various parameters to maximize system performance.

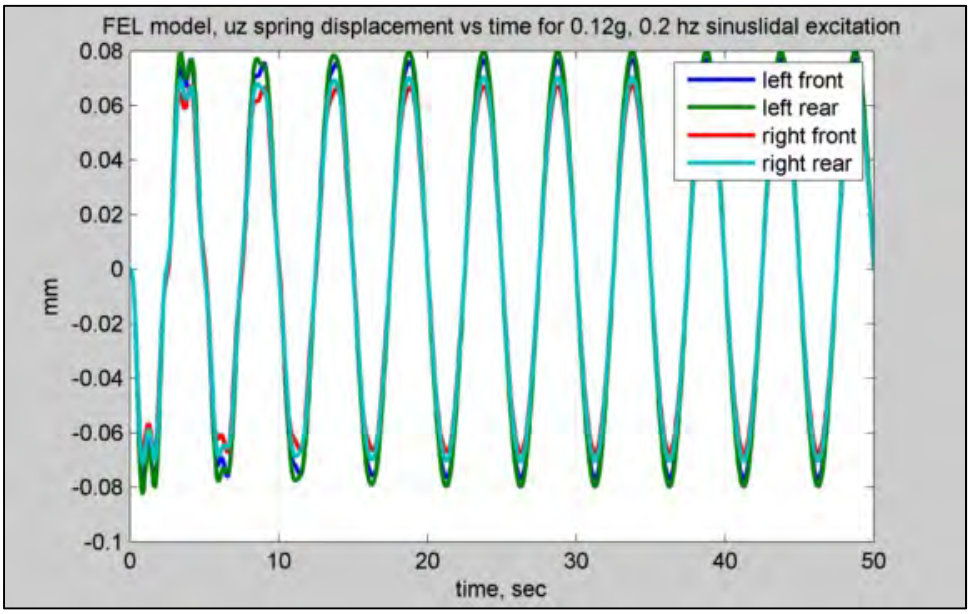

Figure 19: Example Motion Plot

IV. SYSTEM DEVELOPMENT

A. INPUT FREQUENCIES

The typical spectrum of frequencies driving the FEL system onboard a ship is in Table 4. This set of frequencies lends itself naturally to an isolation frequency of 1 Hz because it is roughly a factor of 4 away from both of the largest amplitude sources of vibration, the waves and the propellers.

Table 4: Environmental Vibrations

Source	Frequency Range (Hz)
Wave Action	< 0.2
Propulsion	4–33 [14]
Electrical Power	60
Auxiliary Machinery	> 60

B. ISOLATION STRATEGY

In order to attain the 1 Hz isolation frequency for the system, the spring constant must be calculated. The natural frequency of the isolation is $f = 2\pi\sqrt{k/m}$, where k is the spring constant in N/m, m is the suspended mass in kg, and f is the natural frequency in Hz; therefore, $k = 4\pi^2 fm$. Since the spring constant depends on the suspended mass, the baseplate design will have to be finalized prior to selecting it.

Assume for the time being that the wave action frequency is ~0.1 Hz. If the isolation frequency is a decade away at 1 Hz, then there is sufficient separation that little to no energy transfer will occur between the excitation and the isolation. The same principle applies between the springs that are suspending the system and the system itself. With an ~1 Hz natural frequency for the springs, designing the baseplate for a ~10 Hz lowest distortion mode will place a decade of separation between it and the springs as well and minimize energy transfer between them.

C. BASEPLATE EVOLUTION

1. Solid Plate

The solid model was created with a ~160 ton, 10 centimeter thick solid steel plate as its base. There was no particular justification for this dimension other than it seemed to be a reasonable starting point. The plate was then transferred to ANSYS and analyzed.

It was determined that a 10 cm solid was inadequate to attain the 10 Hz or greater lowest distortion frequency desired. This simulation also revealed that the first distortion mode for this structure would be a bending mode and the second mode would be torsional; these mode shapes are shown in Figure 20. Several iterations later, it was determined that in order to achieve ~10 Hz, the baseplate would need to be 1 meter thick and weigh nearly 1600 tons.

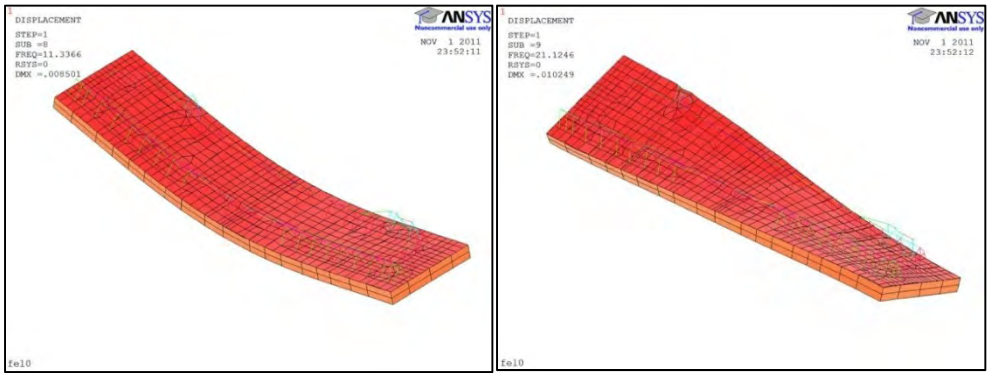

Figure 20: First Bending Mode (Left), First Torsional Mode (Right)

2. Simulated I-beams

A weight of 1600 tons is quite large for a single piece of equipment, so a better strategy for baseplate design would be necessary. A hand calculation revealed an I-beam array structure that has ~95% of the bending stiffness of the solid plate, and has only ~20% of the mass. Adding this into the ANSYS model as a lower density for steel and optimizing for first bending and torsional mode frequencies lead to an ~150 ton structure that would perform as desired. There are, however, a couple of issues with this structure.

First, 150 tons is still heavier than it likely needs to be. Second, there is a reduction of torsional stiffness that arises from that use of I-beams that is not accounted for when simulating in this manner.

3. Box Baseplate

In continuing the development of the baseplate, a box structure was devised so that an accurate accounting of the internal structure could be achieved. The internal structure can be seen in Figure 21. To reduce overall system mass, the construction material was changed to aluminum. The model of this structure was set up so that a design study varying multiple parameters could be performed and an optimum could be selected. The thickness of the ribs, the thickness of the top and bottom plates, and the overall height of the structure could be varied individually while tracking the first bending and torsional mode frequencies and the mass of the system.

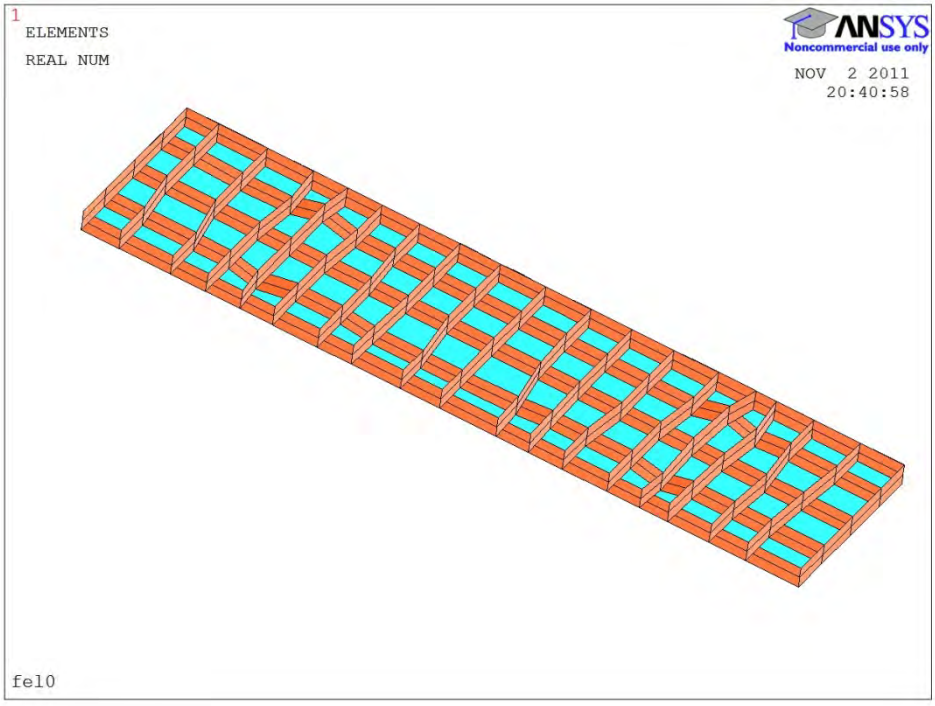

Figure 21: Box Baseplate Internal Structure

A parametric study was performed varying the rib, top and bottom plate thicknesses from 1 to 10 cm in 1 cm increments. Also, the box height was varied from 50 to 150 cm in 10 cm increments. The results are in Figure 22, showing two points for each combination: one for the first bending mode and first torsional mode frequency versus the mass. From this plot, there emerges an easy selection for the system design, the rightmost of the three lowest points in the bending category. This case has a mass of ~55 tons, a top and bottom thickness of 4 cm and a height of 1 m.

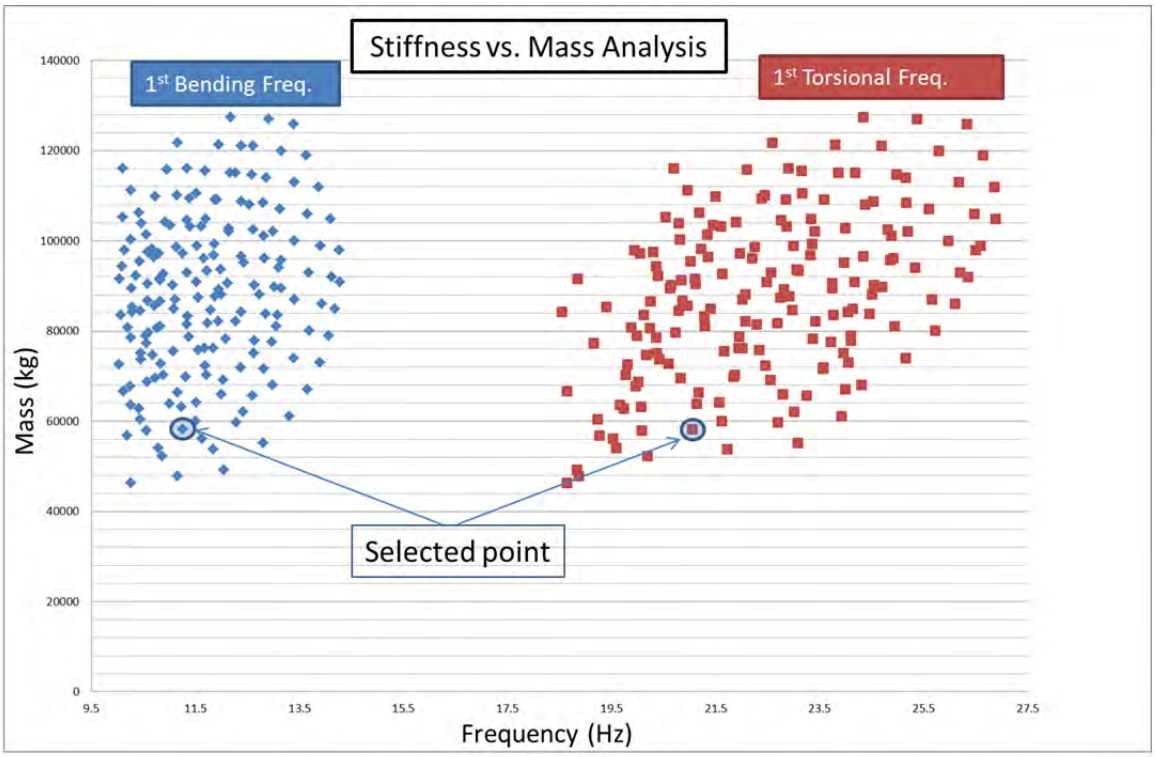

Figure 22: Box Baseplate Parametric Study Results

This more practical structure led the design into another situation with problems. The intent was to minimize the system mass while attaining at least 10 Hz for the first bending mode, and as much separation between bending and torsional frequencies as possible. The heavier components, such as the linear accelerator cryo-modules and the beam dump, pull on the top plate at the mounts hard enough to deform it. This

deformation leads to excessive motion in the beam line and larger displacements for all of the components mounted to the bedplate. Figure 23 shows an exaggerated example of this type of deformation.

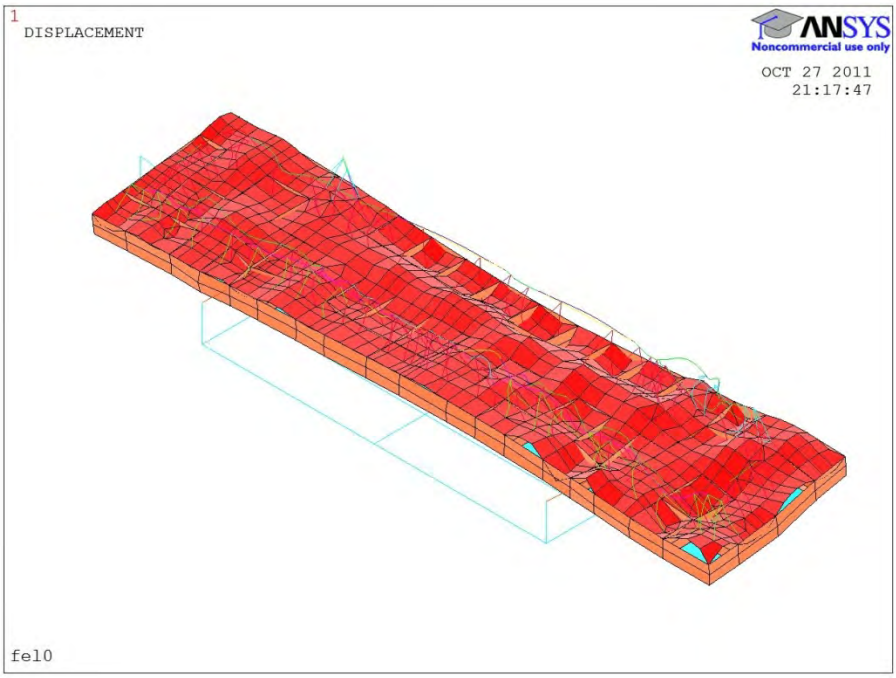

Figure 23: Distorted Surface from Insufficient Top Plate Thickness

To avoid significant top-plate deformation, the top plate needed to be at least 5 cm thick. The extra thickness added enough additional stiffness so that the overall height of the baseplate could be reduced in order to lower the mass while maintaining sufficient performance. With the thicker top and bottom, 20 cm could be taken out of the height of the baseplate while keeping the 2 cm ribs and still maintaining the system performance. This resulted in the first bending mode occurring at 11.33 Hz, with the first torsional mode occurring at 21.12 Hz, and a mass of 58.2 metric tons. This combination is only 3 tons heavier than the previous solution.

D. SIMULATED SHIP STRUCTURE

The starting point for the ship structure is shown in Figure 24. For this project, it is being assumed that the deformation of the ship's hull will have little effect on a

resiliently isolated structure. Because of this, the simulated ship structure will be set up to minimize energy dissipation in it and ensure as much of the input as possible is transferred to the isolation system. This structure is constructed of beams that have effectively no mass and infinite stiffness so that it will not deform. In the center of the structure there is a mass node, an element with no volume that can be set to any mass needed. In this model it is set to 1000 times the mass of the rest of the system to ensure the motion of the suspended system does not cause a resonance in the mass node. This mass and beam combination will facilitate using the ship's structure as a shaker table by applying motion to the mass node and translating that motion through rigid beams to the isolations. Four springs were used as a starting point in the vertical (Z) axis positioned ~1 m in from the outside edge of the baseplate, directly under the beam line, on the node line. The node line is a line that does not move when the system is excited in the first bending mode. In this case it is located ~25% of the way in from both ends of the long (X) axis. Two more springs were used equidistant from the geometric center normal to the X axis, and one additional spring was used normal to the short (Y) axis. The idealized spring constants were calculated using the system mass determined earlier, the number of springs for a given axis, and the 1 Hz isolation frequency.

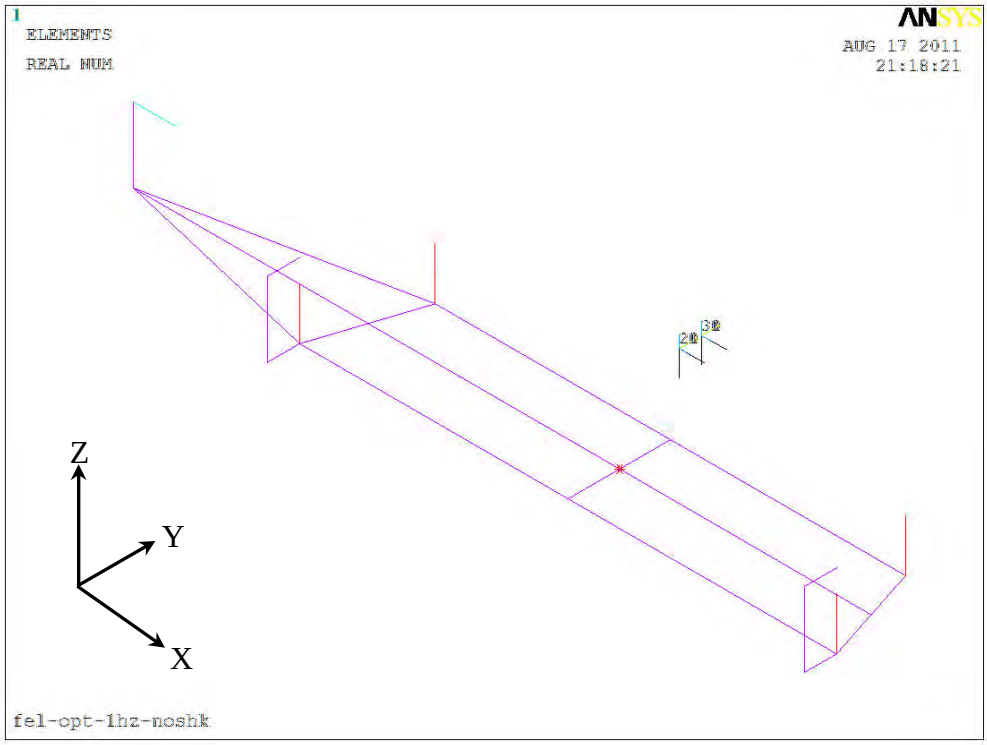

Figure 24: Initial Simulated Ship Structure

Figure 25 shows the frequency response behavior of the mass node. This proves that the ship structure is sufficiently rigid, and the mass node is heavy enough to evenly convey the forcing function to the isolators without distorting or resonating it. If there were any nonlinearaties in this plot, the stiffness of the rigid beams or the mass of the mass node would have to be increased.

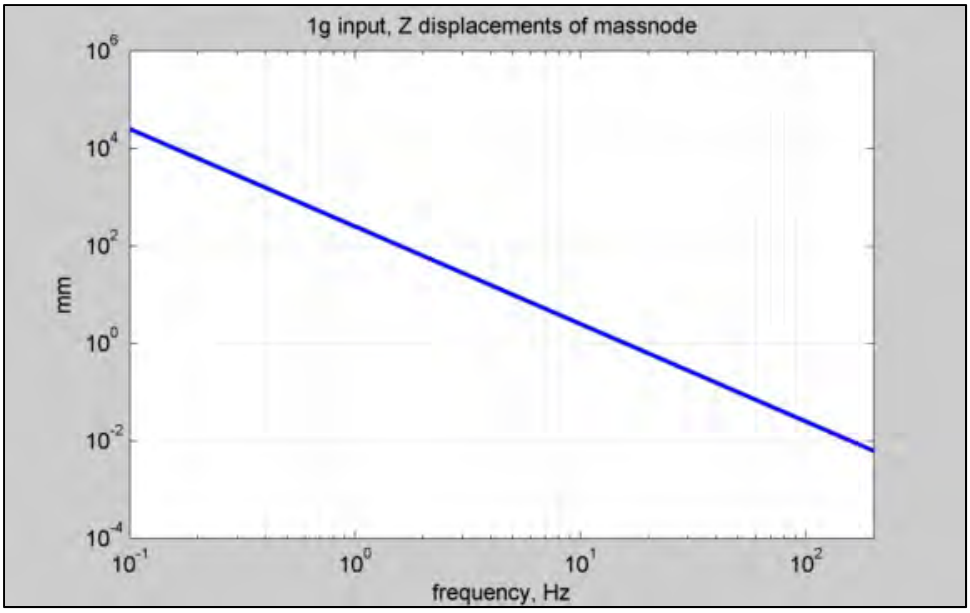

Figure 25: Mass Node Z Displacement vs. Frequency

In this design, there is a significant difference in mass between the cryo module side of the FEL system and the optical resonator side. This difference generated a significant roll motion about the X axis which will need compensation. A first attempt to reduce this roll motion was made by moving the mounting location of the springs from below the beam line to the outer edge of the baseplate. Figure 26 shows the X direction motion of the left and right side mirrors relative to the undulator. From the figure it can be seen that the displacements have gotten about 10% smaller. This 10% reduction follows through most of the parameters being tracked by the model.

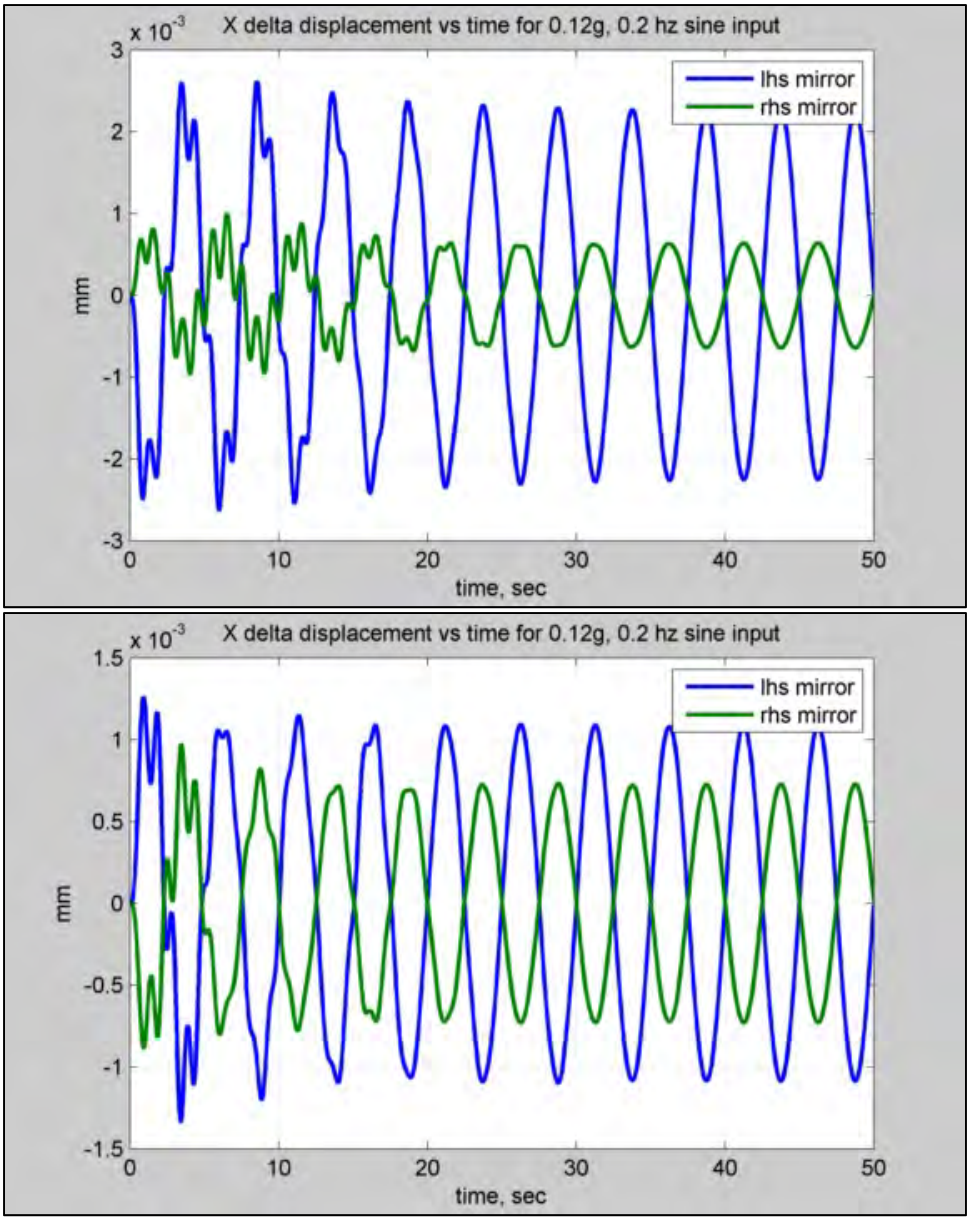

Figure 26: X-Direction Mirror Displacement Before (Top) and After (Bottom) Moving Mounts

Consulting with the engineers at CSA-MOOG Engineering led to the selection of an off-the-shelf Firestone air spring to use as an isolator. These springs can support a static load of about 30 tons and have a spring constant of about 263 kN/m. Based on the mass determined for the baseplate, 1 Hz isolation requires a spring constant of 2.33×10^6 kN/m. This means that 9 of these springs would be the closest match to the ideal case.

Considering that 9 springs is an odd number of real springs required, the model which only contained 4 springs was run with different spring constants on either side to simulate 9 springs and determine if the asymmetry would be beneficial or if 10 springs should be used. This step is being performed because it is far simpler to adjust a spring constant than to set up the ship structure to support more springs. This model was run with the greater spring constant on either of the long sides of the model. The roll motion, and the movement of the components attached to the baseplate, was worse with more springs under the lighter side. As expected, the greater spring constant under the heavier side further improved the system performance. The relative motion of the mirrors in the X-direction is shown in Figure 27, and shows a further reduction of relative motion between the two mirrors (forming the optical resonator) and the undulator.

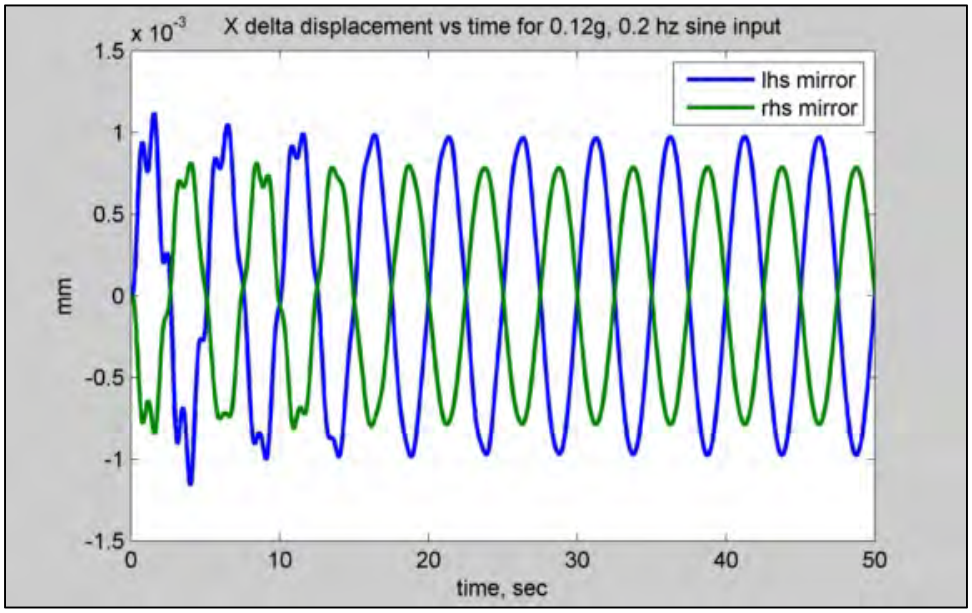

Figure 27: X-Direction Mirror Displacement of Final Configuration

Due to the success of the simulation of 9 springs, another model ship hull was created. This model had the 9 springs evenly spaced at the outer edge of the baseplate with 4 under the optical resonator and 5 under the heavier side. Since this model was only being excited in the vertical direction, the horizontal springs could continue to be

modeled as the ideal springs from the initial model. Figure 28 is the final ship structure on which the FEL system is mounted. It shows the vertical springs highlighted in green, the horizontal ones highlighted in red, and that more beams have been added to the structure to ensure deflections of the spring mounts are not introduced by asymmetries in spring location.

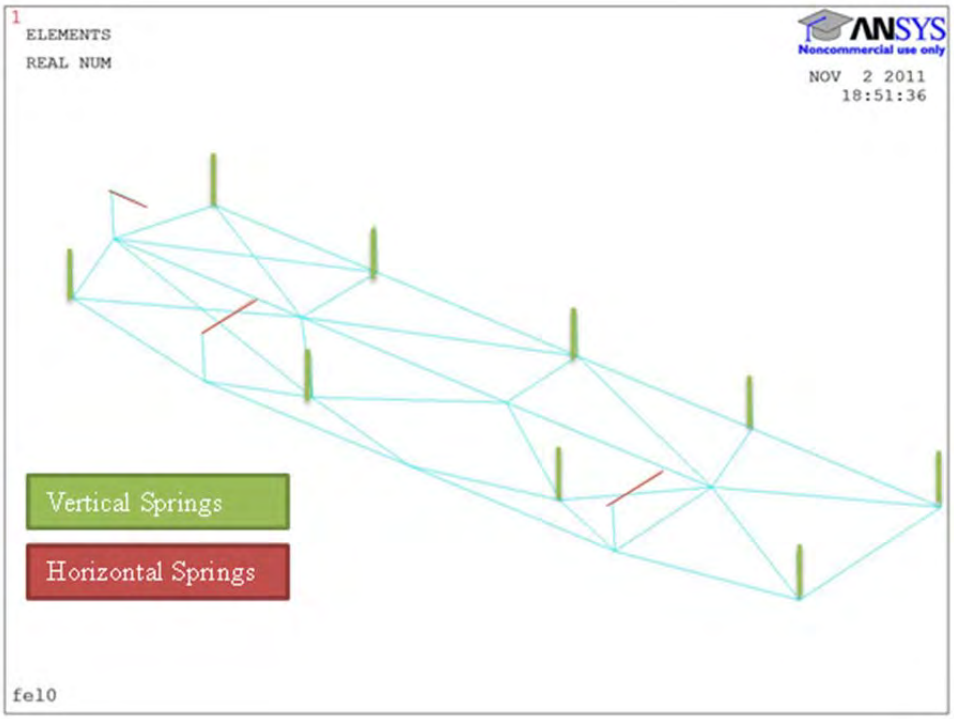

Figure 28: Final Simulated Ship Structure

THIS PAGE INTENTIONALLY LEFT BLANK

V. SIMULATION RESULTS

A. BASEPLATE MOTION

The final configuration of the model was subject to both wave motion and shock. The resulting overall baseplate motion due to the sea input is shown in Figure 29 and shock is shown in Figure 30. The sea state 6 (SS-6) response resulted in about 60 mm of total travel with a period of ~5 s and some higher frequency transients that have periods of ~1 s. This travel approximately matches the linear response region of the selected air spring, and reinforces the likeliness that an actual system would perform as predicted by a linear model. The underwater (UW) explosion results are favorable as well. The springs are capable of a total motion of about 38 cm and under the worst-case input the system travels ~34 cm. The shock response produces motion with a period of ~1 s with no noticeable higher frequency components, and damps out at about 10% per second. This is desirable because there will not be an additional shock input as the spring reaches the end of its allowable travel and stops suddenly.

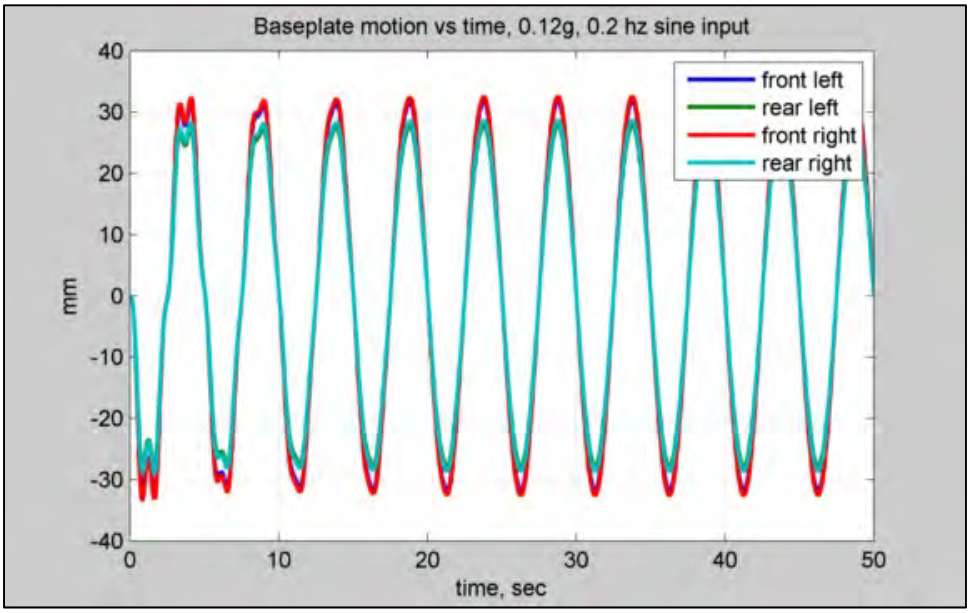

Figure 29: Baseplate Vertical Motion in Response to SS-6

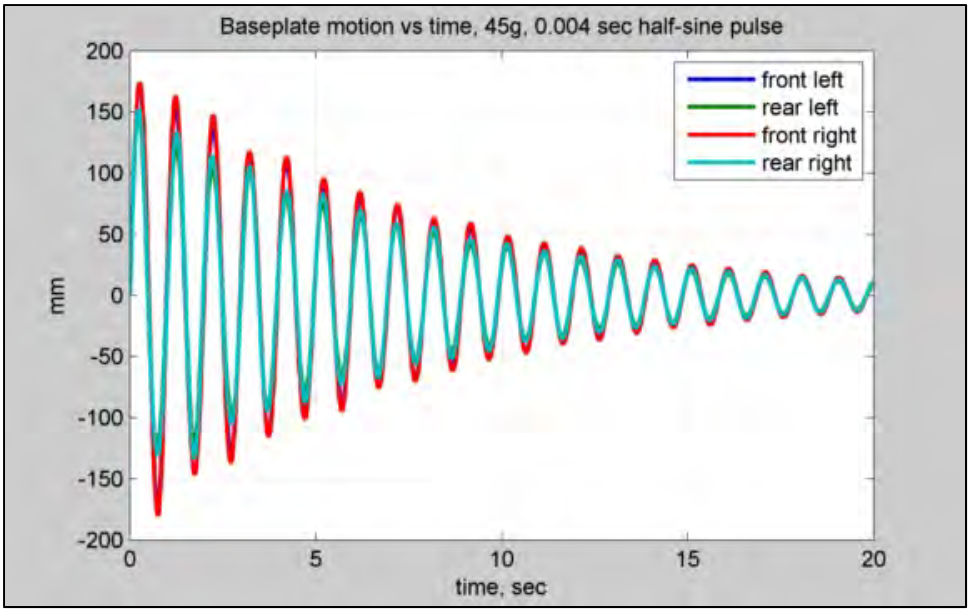

Figure 30: Baseplate Vertical Motion in Response to UW Explosion

B. MIRROR ANGLE

The angle of each mirror with respect to the central axis of the undulator was analyzed. Figure 31 shows an illustration of the mirror angle θ that is being referred to in this section. The magnitude of mirror angular motion is summarized in Table 5. The following figures show the total angle between the undulator axis and the mirror axis. This angle is generated from rotations about the two non-symmetrical axes of the undulator. Figure 32 shows how the right mirror responds to the seas. It has the ~2.5 s period motion that is common in the steady state SS-6 responses in this model; it also has ~0.5 s period components that are caused by the out of phase responses from the two source rotations. Figure 33 shows how the left mirror responds to the seas. It has the same ~2.5 s motion as the right mirror but the higher frequencies are not as significant because the magnitude is about an order of magnitude greater. Figure 34 shows how the right mirror responds to the shock. It has the ~0.5 s motion as well but it shows how this mirror takes ~6 s to build up energy and begin to decay away. Figure 35 shows how the left mirror responds to the shock. It has the ~0.5 s motion again but in this case there is a beating phenomenon that is likely due to the beam dump base structure not being

sufficiently rigid. The imbalances in the FEL system begin to become apparent in these plots. The left mirror, which is on the same side of the system as the beam dump, moves about one order of magnitude more than its twin on the opposite side. The table shows the peak values for the response to shock input and the steady state values for the continuous input once the startup transient subsides. The tolerance on the mirror angle is 0.5 µrad. Additional controls will be needed to control the mirror angle.

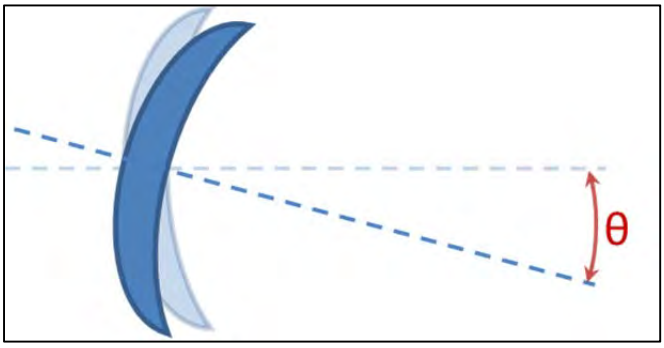

Figure 31: Illustration of Mirror Angle

Table 5: Mirror Angle Results

Mirror	SS-6	UW explosion
Left	82 µrad	700 µrad
Right	3.8 µrad	160 µrad

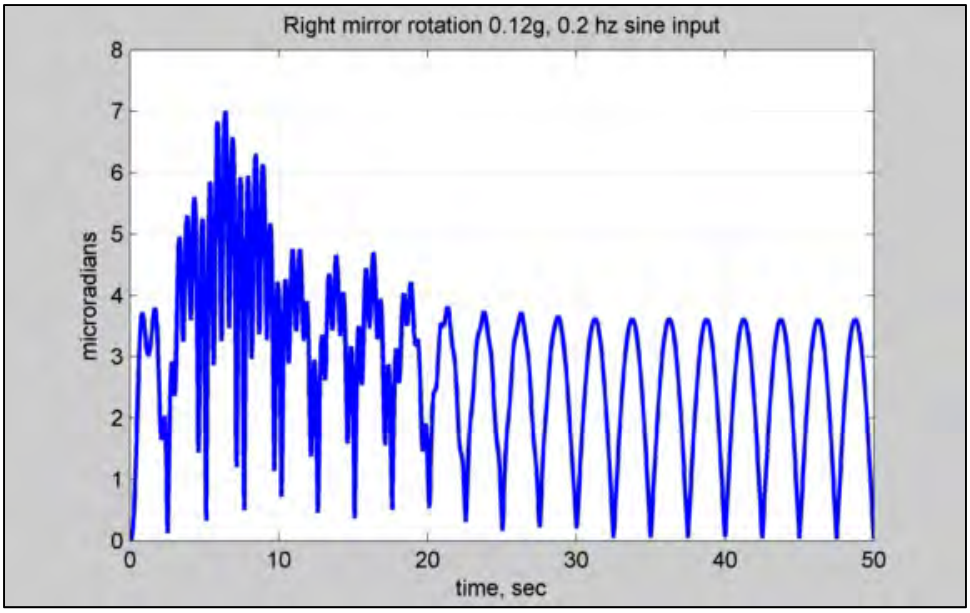

Figure 32: Right Mirror Angular Deflection in Response to SS-6

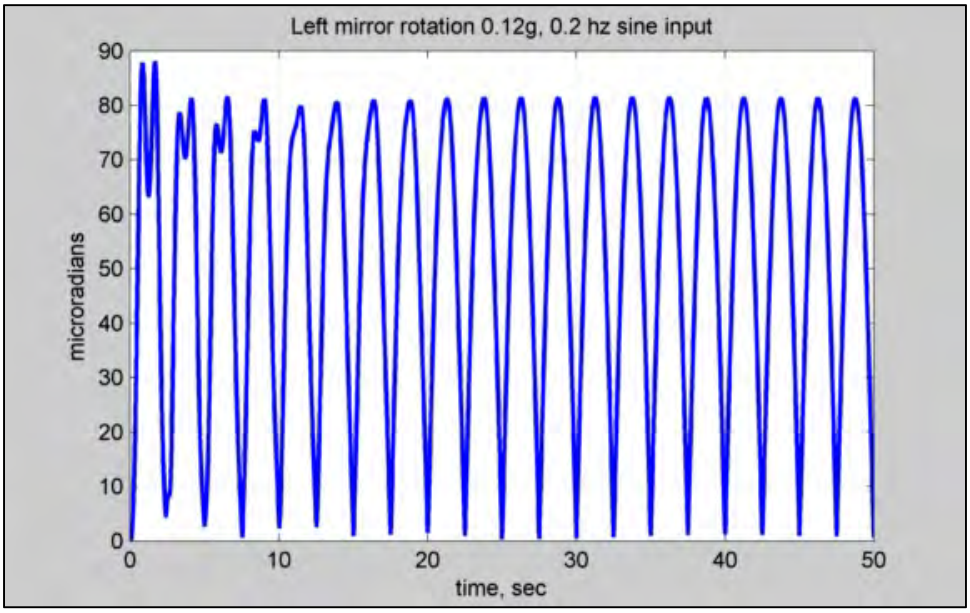

Figure 33: Left Mirror Angular Deflection in Response to SS-6

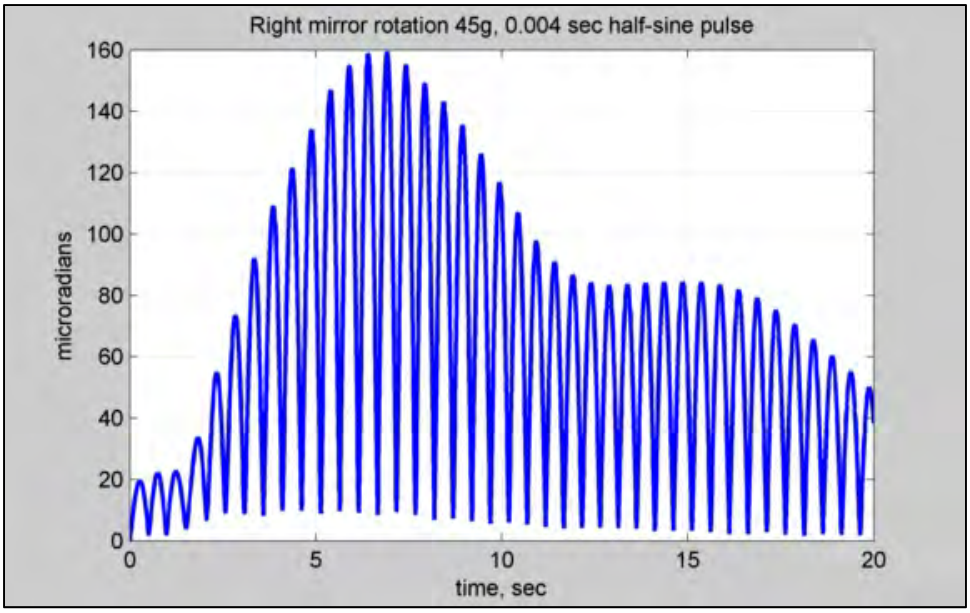

Figure 34: Right Mirror Angular Deflection in Response to UW Explosion

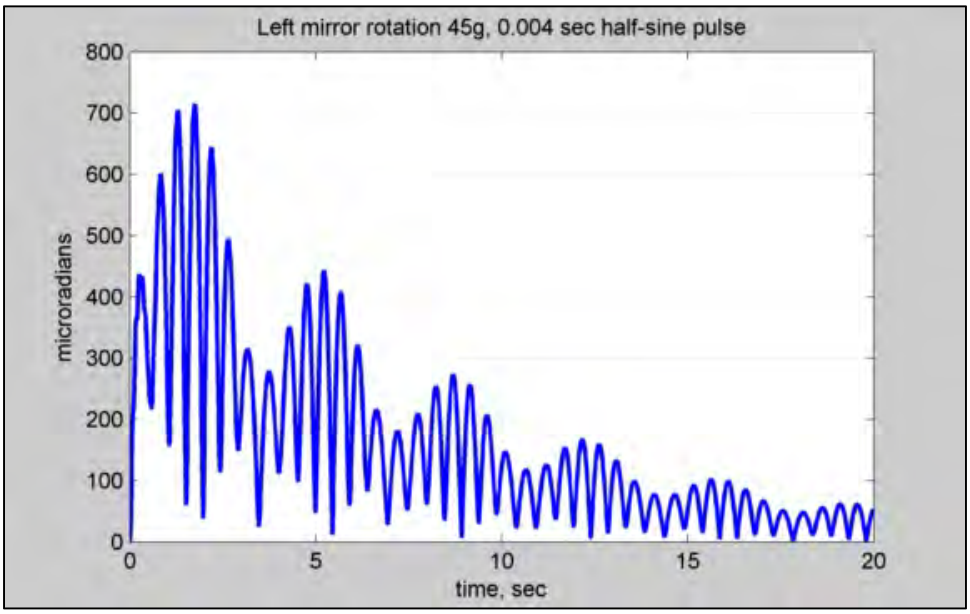

Figure 35: Left Mirror Angular Deflection in Response to UW Explosion

C. MIRROR SHIFT

The shift of each mirror in the plane normal to the central axis of the undulator was analyzed. An illustration of this shift (L) is shown in Figure 36; its magnitude is summarized in Table 6. Figure 37 shows how both of the mirrors respond to the seas. The shift is only a function of a single dimension and as such the short period motions occur at ~1 s vice the 0.5 s motion from the mirror angle results. Figure 38 shows how both of the mirrors respond the shock. The shock results show the same ~1 sec motion as the sea results and the beating caused by the beam dump are present again. The imbalances between the left and right sides of the FEL system continue to pose problems by causing the left side to move more than the right. The differences in the translation motions are not as severe as the angular ones; in this case the difference is closer to a factor of ~2. The tolerance on mirror shift is 50 μm; so that additional controls will be needed to control the mirror position. An active control system will have to reduce the effect of the shock by moving the mirrors by several millimeters in a about a tenth of a second to keep the system in operation.

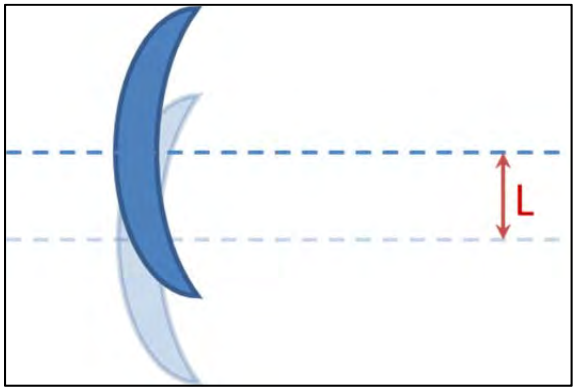

Figure 36: Illustration of Mirror Shift

Table 6: Mirror Shift Summary

Mirror	SS-6	UW explosion
Left	1.2 mm	7.8 mm
Right	0.8	4.4 mm

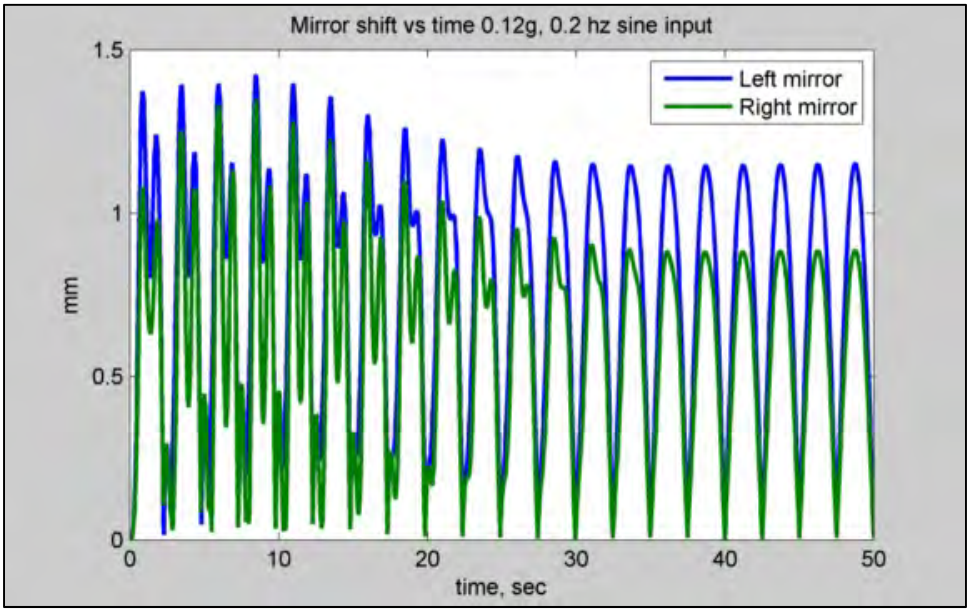

Figure 37: Mirror Shift in Response to SS-6

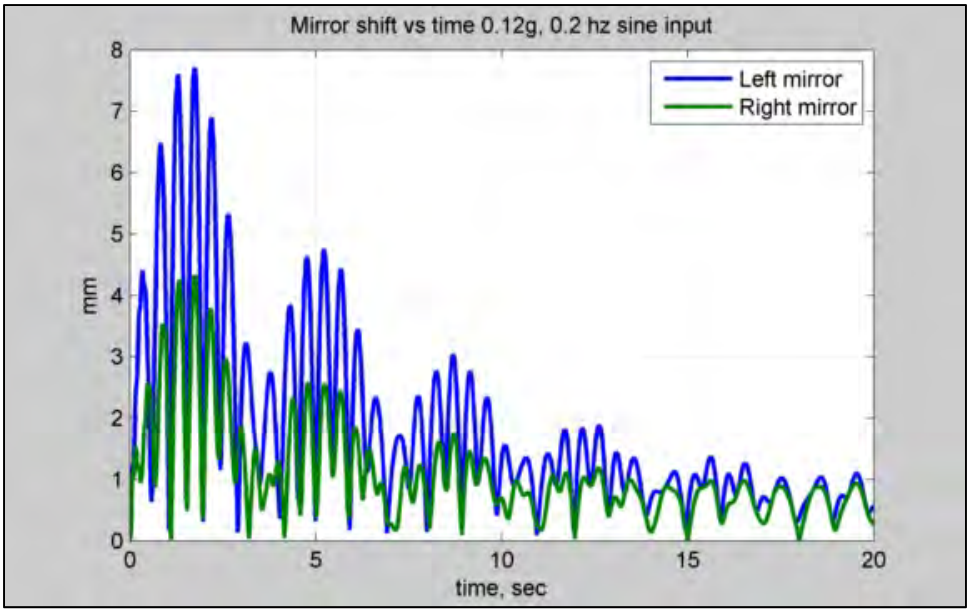

Figure 38: Mirror Shift in Response to UW Explosion

D. OPTICAL PATH ANGLE

The angle θ between the line connecting the two mirrors and the central axis of the undulator was also analyzed. Figure 39 shows an illustration of the angle θ that is being referred to in this section. The seas deflect this angle 26 μrad while the UW explosion deflects it 460 μrad. Figure 40 shows the sea response of the optical path angle. It has the usual ~2.5 s motion as well as the ~1 s shorter period motion and a small amount of the ~0.5 s motion in the first 5 s. The shorter period motion is not very significant in these results because of the larger amplitudes of the rotation. Figure 41 shows the shock response of the optical path angle. It again displays the ~3.5 s beating that is likely due to the beam dump's weight and structure. SS-6 moves the optical path by ~26 μrad off axis, while the UW explosion moves it 460 μrad. The tolerance on this motion is 1 mrad; the control system on the model is sufficient to maintain this parameter in tolerance.

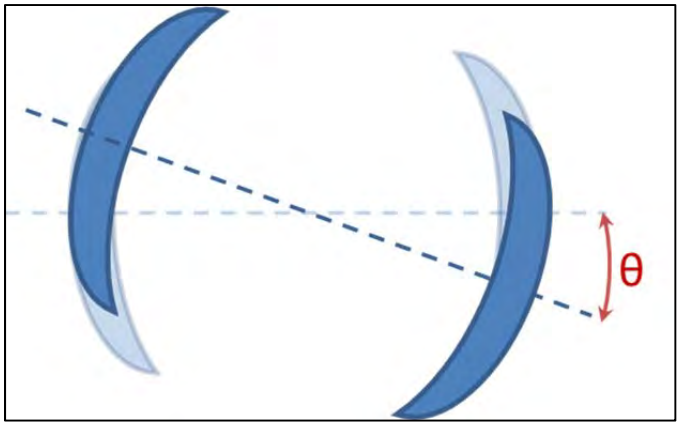

Figure 39: Illustration of Optical Path angle

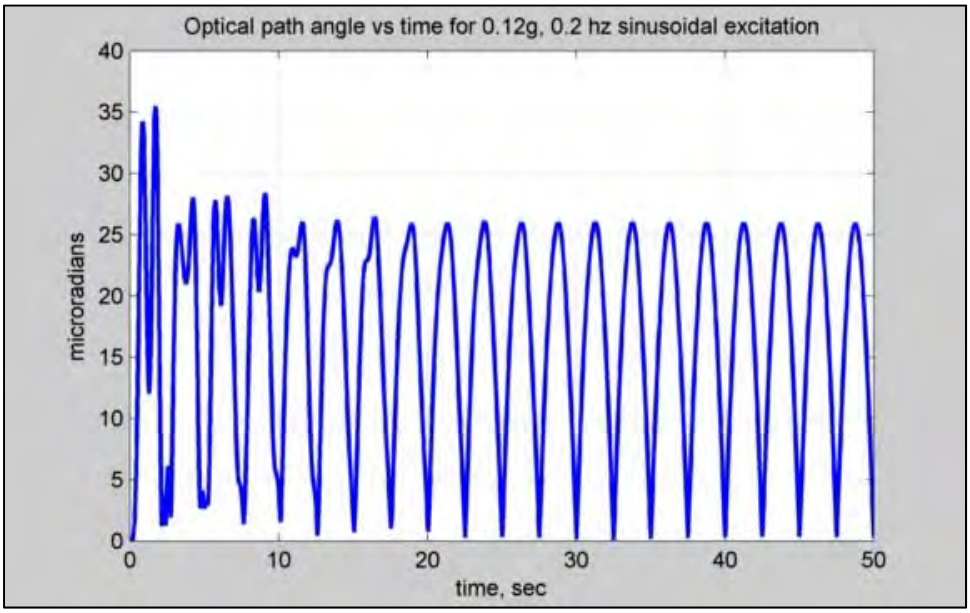

Figure 40: Optical Path Angular Response to SS-6

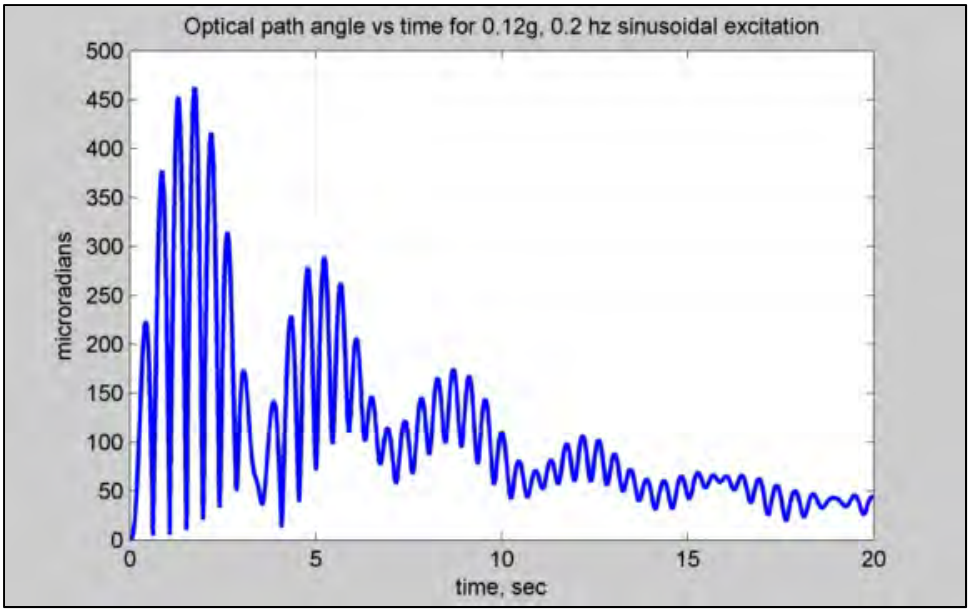

Figure 41: Optical Path Angular Response to UW Explosion

E. OPTICAL PATH SHIFT

The motion in the plane normal to the central axis of the undulator of the line connecting the two mirrors was analyzed. Figure 42 shows an illustration of the shift L that is being referred to in this section. Figure 43 shows the sea response of the optical path shift. It is only slightly affected by the ~1 s motion before it transitions to the steady state ~2.5 s period motion. Figure 44 shows the shock response of the optical path shift. It is done with any transient behavior in the first 2 s and then the amplitude decays away at ~10% per second. The optical path is shifted ~0.4 mm off axis by SS-6 and ~2.3 mm by the shock. The tolerance here is 0.6 mm; the system will be out of tolerance for about ~15 sec during an UW explosion without active controls, but the passive controls in this model will be sufficient during operations up to SS-6. An active control system will have to reduce the effect of the shock by moving the mirrors a few millimeters in about a tenth of a second to keep the system in operation.

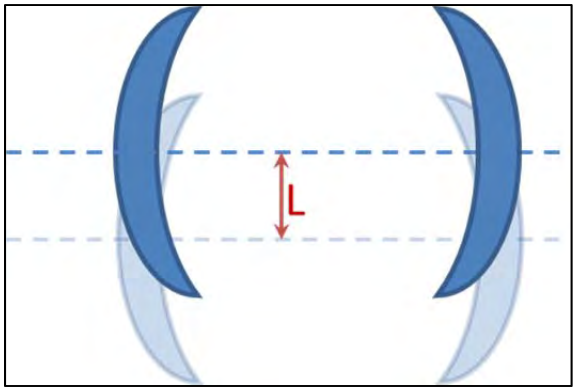

Figure 42: Illustration of Optical Path Shift

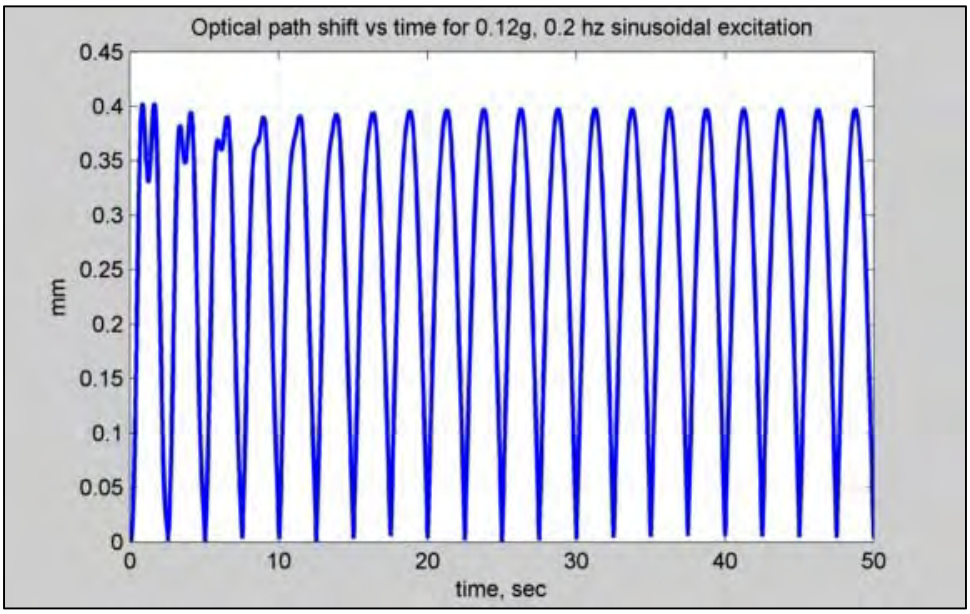

Figure 43: Optical Path Shift Response to SS-6

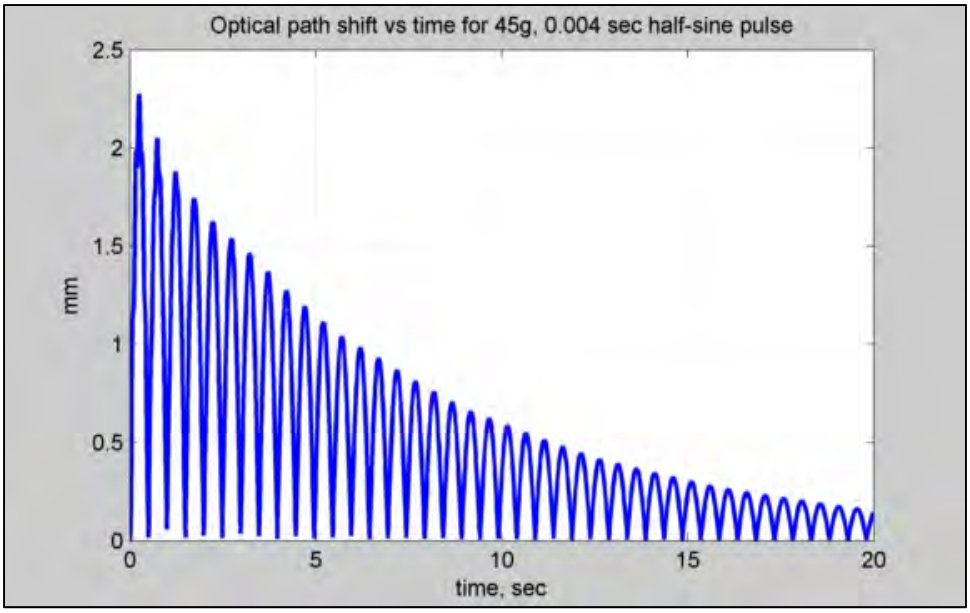

Figure 44: Optical Path Shift Response to UW Explosion

F. RESONATOR LENGTH

The change of length of the resonator was analyzed. Figure 45 shows an illustration of the length L that is being referred to in this section. Figure 43 shows the resonator length behavior in SS-6 waves. The 1 s motion persists through the first 10 s of operation and then the steady state behavior is established. Figure 44 shows the resonator length behavior during an UW explosion. The high frequency behavior subsides in the first 2 s and then the ~2.5 s motion decays away at ~10% per second. Under SS-6 input the resonator grows and shrinks by about 90 μm. Under UW explosion the resonator grows and shrinks by about 500 μm but returns to the SS-6 value in about 30 s. The tolerance on this motion is 0.5 μm and is essential for maintaining the FEL in operation. Further control will be needed but this model provides an operational envelope in terms of period and amplitude in which the active control system must operate.

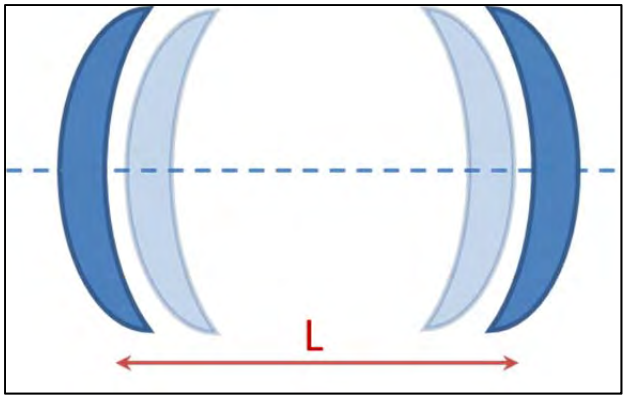

Figure 45: Illustration of Resonator Length

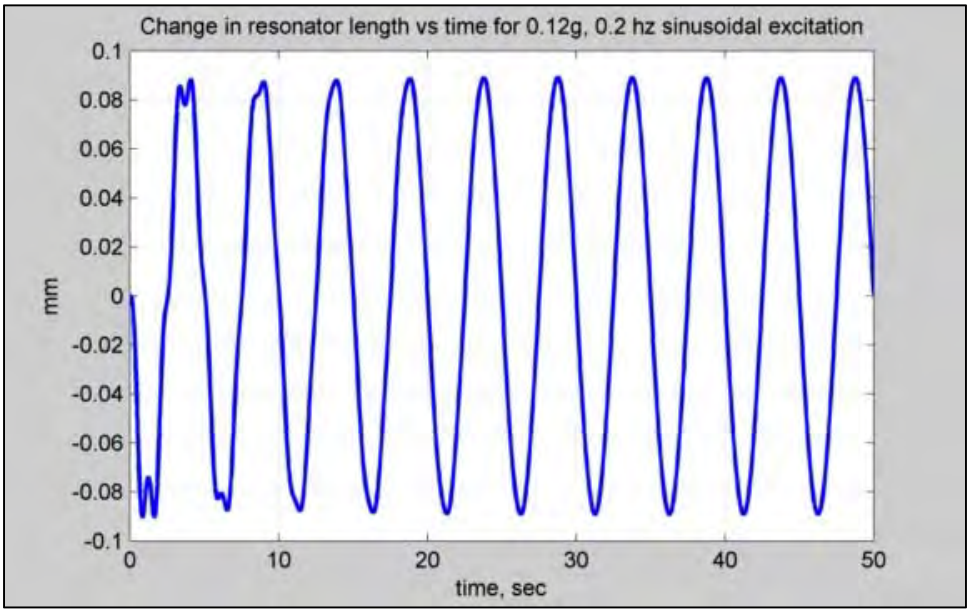

Figure 46: Resonator Length Response to SS-6

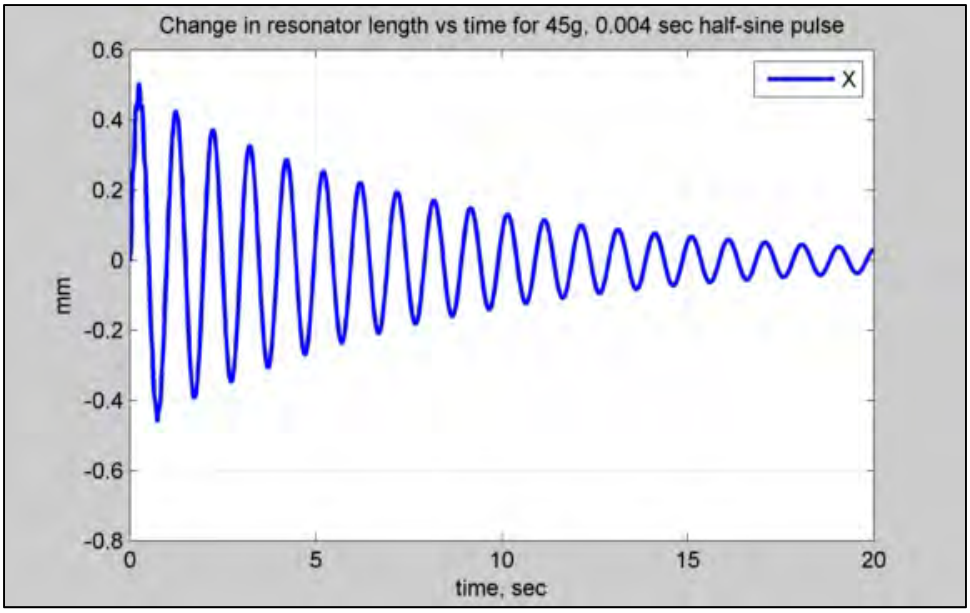

Figure 47: Resonator Length Response to UW Explosion

VI. CONCLUSION

A. CONCLUSION

The tolerances and worst-case result for sea state 6 (SS-6) waves and under water (UW) explosion are summarized in Table 7, with out of tolerance values in red. Three out of the 5 figures of merit developed in this project are not in tolerance for the worst-case scenarios chosen. The other sea-states were also explored to show how the system behavior changed with weakening seas as shown in Table 8. All of the parameters being monitored show significant decrease with sea-state but only mirror shift changes to being in tolerance and that only happens in sea-state 3.

Table 7: Tolerances and Simulation Results

Dimension to be Controlled	Tolerance	Model Prediction for Sea State 6	Model Prediction for Under Water Explosion
Mirror Angle	±0.5 µrad	80 µrad	700 µrad
Mirror Shift	±50 µm	1.4 mm	8 mm
Optical Path Angle	±1 mrad	26 µrad	460 µrad
Optical Path Shift	±0.6 mm	400 µm	2.3 mm
Mirror Separation	±0.5 µm	90 µm	500 µm

Table 8: Simulation Results for Varied Sea States

Sea State / Dimension	6	5	4	3
Mirror Angle	80 µrad	34 µrad	2.2 µrad	3.4 µrad
Mirror Shift	1.4 mm	480 µm	90 µm	48 µm
Optical Path Angle	26 µrad	12 µrad	2 µrad	1.1 µrad
Optical Path Shift	400 µm	160 µm	33 µm	16 µm
Mirror Separation	90 µm	38 µm	7 µm	3.8 µm

The passive control system laid out in this project is not able to maintain the FEL system components in alignment sufficiently to allow for its operation. An active control system will be required. This system does, however, reduce the amplitude of motions that the active control system must be able to control.

Typical active controls systems operate in the kHz range and all of the motions in this system that need to be controlled are in the 0.5 to 5 Hz range. This, combined with the reduced amplitudes of motion from the passive isolation system, make it likely that the FEL system can be operated successfully onboard ships.

The goal of this project was not to develop a passive isolation system that would enable FEL operation on board a ship. It was to develop a system that would reduce the amplitude of the vibrations left to active controls to a reasonable level and to establish the operating envelope for that system. Both goals have been successfully achieved.

B. FUTURE WORK

To improve this model, several steps can be taken in the future. Adding active controls to the air springs, such as a voice coil actuator, would greatly improve performance and would be closer to the system that will be installed on a ship. Furthermore, a more complete model of the ship's hull could be added that would allow for the addition of the effect of hull bending on the model. Also, there are many FEL system components such as RF power and the cryo plant that were assumed not to be on the baseplate. Either adding them onto the baseplate or modeling their connections will be important in a better model. Finally, once the shipboard FEL system design matures to the point that no further major structural changes are going to be made, that model should be incorporated into this project.

LIST OF REFERENCES

[1] Paul Schafer Institute, "SwissFEL Accelerator Design," [Online]. Available: http://www.psi.ch/swissfel/swissfel-accelerator. [Accessed 29 8 2011].

[2] Defence News, "Global Media Applications," 21 01 2011. [Online]. Available: http://globaldefencemedia.com/news_daily/21_01_2011/FEL_program.html. [Accessed 29 8 2011].

[3] Dassault Systèmes SolidWorks Corp, *SolidWorks,* Waltham, 2011.

[4] German Electron Synchrotron, "Photon Science," Helmholtz, [Online]. Available: http://hasylab.desy.de/facilities/flash/machine/how_it_works/high_gain_fel/index_eng.html. [Accessed 29 8 2011].

[5] W. Colson, *PH4055 "Free Electron Lasers,"* Montrerey, California, 2011.

[6] B. Colson, T. Schriempf, J. Blau, K. Cohn and B. Rusnak, "MW Class FEL Real-Time Performance Optimization," in *DEPS FEL Conference*, Broomfield, 2010.

[7] J. Blau, W. Colson, R. Edmonson, R. Neuerman and M. Stanton, "Electron Beam Quality and Stability Effects in Free Electron Laser Amplifiers and Oscillators," Physics Department, Naval Postgraduate School, Monterey, 2009.

[8] Advanced Energy Systems, Inc., *FELSIM,* Medford, 2011.

[9] ANSYS Inc., *ANSYS,* Canonsburg, 2010.

[10] World Meteorological Organization, Guide to Meteorological Instrumentsand Methods of Observation, Geneva: World Meteorological Organization, 2008.

[11] Y. S. Young and N. A. Schneider, "Ship Shock Trial Simulation of USS Winston S. Churchill (DDG 81): Modeling and Simulation Strategy and Surrounding Fluid Volume Effects," Naval Postgraduate School: Department of Mechanical Engineering, Monterey, 2003.

[12] R. F. Beck and A. W. Troesch, *SHIPMO,* Ann Arbor, 1989.

[13] The MathWorks Inc., *MATLAB,* Natick, 2011.

[14] Naval Sea Systems Command, *MIL-STD-167–1(SHIPS): Mechanical Vibrations Of Shipboard Equipment*, Department of the Navy, 1974.

INITIAL DISTRIBUTION LIST

1. Defense Technical Information Center
   Ft. Belvoir, Virginia

2. Dudley Knox Library
   Naval Postgraduate School
   Monterey, California

3. William B. Colson
   Naval Postgraduate School
   Monterey, California

4. Fotis Papoulias
   Naval Postgraduate School
   Monterey, California

5. Keith R. Cohn
   Naval Postgraduate School
   Monterey, California

6. Michael R. Hatch
   Mountain View, California

7. Mike Evert
   CSA Engineering
   Mountain View, California